iScience

CellPress
OPEN ACCESS

Article

Melatonin alleviates high-fat-diet-induced dry eye by regulating macrophage polarization via IFT27 and lowering ERK/JNK phosphorylation

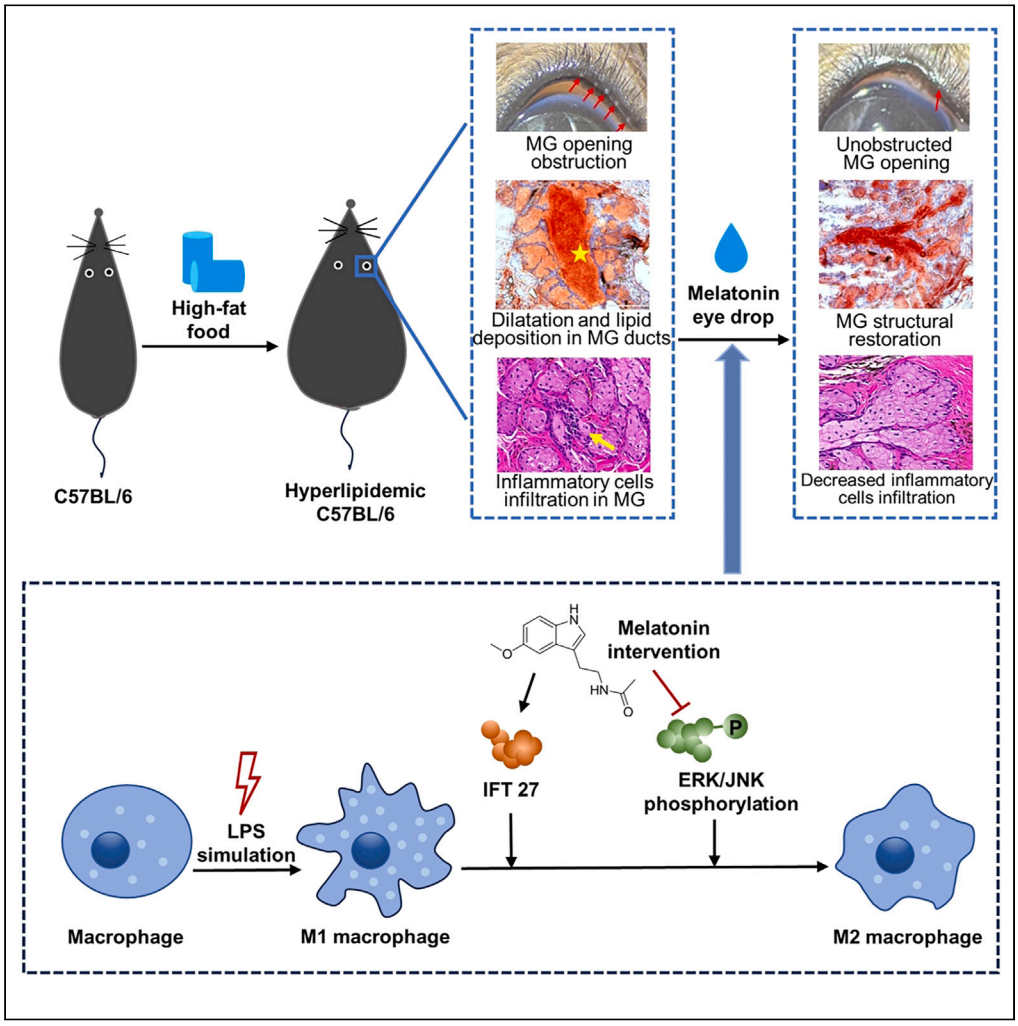

Yuying Cai, Xin Zhang, Chuanxi Yang, Yaping Jiang, Yihui Chen

ellenjyp@163.com (Y.J.)
1300089@tongji.edu.cn (Y.C.)

Highlights

High-fat diet disturbs ocular surface microenvironment by inducing inflammation

Melatonin restores the secretory function of meibomian and lacrimal glands

Melatonin upregulates M2/M1 macrophage ratio, and exert anti-inflammatory effects

Melatonin regulates macrophage polarization via IFT27 and ERK/JNK phosphorylation

Cai et al., iScience 27, 110367
July 19, 2024
https://doi.org/10.1016/j.isci.2024.110367

iScience

CellPress
OPEN ACCESS

Article

Melatonin alleviates high-fat-diet-induced dry eye by regulating macrophage polarization via IFT27 and lowering ERK/JNK phosphorylation

Yuying Cai,[1,3] Xin Zhang,[1,3] Chuanxi Yang,[2] Yaping Jiang,[1,*] and Yihui Chen[1,4,*]

SUMMARY

Dry eye disease is the most common ocular surface disease globally, requiring a more effective treatment. We observed that a high-fat diet induced macrophage polarization to M1 and further induced inflammation in the meibomian and lacrimal glands. A four-week treatment with melatonin (MLT) eye drops can regulate macrophage polarization and alleviate dry eye signs. To investigate the therapeutic effects and mechanisms of action of MLT on high-fat-diet-induced dry eye disease in mice, RAW 264.7 cells pretreated with LPS and/or MLT underwent digital RNA with the perturbation of genes sequencing (DRUG-seq). Results showed that IFT27 was up-regulated, and MAPK pathways were suppressed after MLT pretreatment. ERK/JNK phosphorylation was reduced in meibomian glands of MLT-treated dry eye mice and increased in IFT27 knockdown RAW 264.7 cells. In summary, MLT regulated macrophage polarization via IFT27 and reduced ERK/JNK phosphorylation. These results support that MLT is a promising medication for dry eye disease.

INTRODUCTION

Dry eye disease (DED) is the most prevalent ocular surface disease globally.[1,2] The ocular surface microenvironment (OSM) consists of the cornea, conjunctiva, meibomian glands (MGs), lacrimal glands (LGs), neural networks, specific cells, matrices, small molecules, and microbiome collaborate.[3] MG and LG secretions are the main components of the aqueous and lipid layers of the tear film and help to maintain clear optical surfaces, protect the eye from microorganisms, and sustain homeostasis.[4–6] MG dysfunction (MGD) is the most common cause of lipid deficiency DED.[7] It is usually characterized by the obstruction of the terminal ducts or abnormalities in the substance or amount of secretion by the glands.[8,9] Hyperlipidemia is a risk factor for MGD.[10,11] The severity of MGD increases with the elevation of serum triglyceride and low-density lipoprotein levels.[12,13] In addition, metabolic diseases such as obesity and hyperlipidemia expose organisms to persistent chronic inflammation,[14] and proinflammatory cytokines can induce apoptosis.[15,16] Mice on a high-fat diet (HFD) exhibit lipid accumulation in MGs, which exacerbates MGD by potentially causing MG cell apoptosis and dysregulating MG physiological functions.[17]

Several types of immune cells are involved in the pathogenesis of dry eye disease and are rapidly recruited at the site of injury.[18] Macrophages are detected in large numbers in specimens from patients with dry eye disease and play an important role in the development and dissipation of inflammation.[19,20] Classically activated M1 macrophages and alternatively activated M2 macrophages are the two most typical phenotypes.[21] M1 macrophages induced by bacterial lipopolysaccharide (LPS) produce proinflammatory cytokines such as interleukin (IL)-6, IL-1β, tumor necrosis factor α (TNF-α), and inducible nitrogen oxide synthase (iNOS). Conversely, IL-4-induced M2 macrophages produce a variety of anti-inflammatory cytokines, including arginase-1 (Arg-1) and IL-10.[22,23] In this study, we found that macrophages are abnormally polarized in the development of dry eye disease; therefore, the modulation of this polarization is a potential treatment strategy. Furthermore, the mitogen-activated protein kinase (MAPK) pathway plays an important role in intracellular signal transduction in eukaryotic cells and is involved in the regulation of cell differentiation, proliferation, division, and apoptosis.[24] Among the MAPK pathways, the transduction pathway was identified first, which is divided into extracellular signal-regulated kinase 1 (ERK1) and ERK2.[25–27] The MAPK signaling pathway promotes the transcription of various inflammatory genes, including genes encoding TNF-α, IL-1β, and COX-2 enzymes, and the activation of transcription factor NF-κB.[28,29] When TNF-α binds to its receptor, the MAPK and NF-kB signaling pathways are activated. This results in the amplification of the inflammatory response, worsening tissue damage.[30]

Melatonin (MLT) is a methoxyindole synthesized and secreted principally by the pineal gland at night under normal light/dark conditions.[31–33] MLT also has strong anti-inflammatory and antioxidant properties and its role in various ophthalmic diseases, including ocular surface disorders, such as DED and MGD, is currently being investigated.[10,34,35] MLT was found to attenuate lipopolysaccharide-induced

[1]Department of Ophthalmology, Yangpu Hospital, School of Medicine, Tongji University, Shanghai, China
[2]Department of Cardiology, Yangpu Hospital, School of Medicine, Tongji University, Shanghai, China
[3]These authors contributed equally
[4]Lead contact
*Correspondence: ellenjyp@163.com (Y.J.), 1300089@tongji.edu.cn (Y.C.)
https://doi.org/10.1016/j.isci.2024.110367

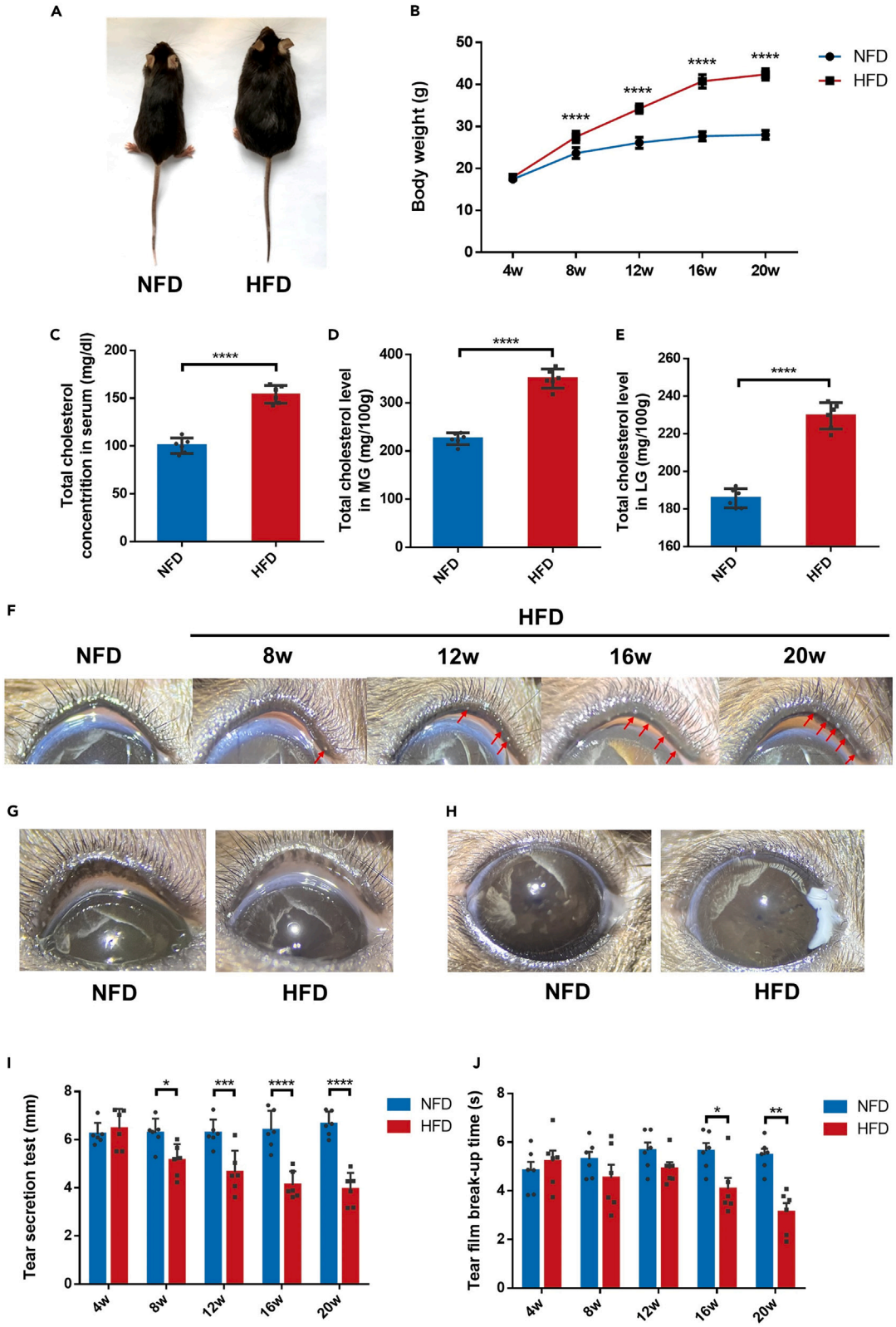
A
NFD
HFD
B
Body weight (g)
NFD
HFD
4w
8w
12w
16w
20w
****
C
Total cholesterol concentrition in serum (mg/dl)
D
Total cholesterol level in MG (mg/100g)
E
Total cholesterol level in LG (mg/100g)
F
NFD
HFD
8w
12w
16w
20w
G
H
I
Tear secretion test (mm)
J
Tear film break-up time (s)
*
**
***

Figure 1. HFD-induced obesity and dyslipidemia, as well as MGD in C57BL/6 mice

HFD mice had larger body size (A) and significant weight gain (B), with total cholesterol level rise in serum (C), MGs (D), and LGs (E). Representative slit-lamp images showed HFD mice exhibited the obstruction of MGs' opening (F, red arrows), depigmentation in lid margins (G), and milky-fluid secretion (H). Tear secretion (I) and tear film rupture time (J) were both significantly decreased in HFD mice. Data are presented as mean ± SD; $n = 6$ per group. A Mann–Whitney U test was used for statistical analysis. *$p < 0.05$, **$p < 0.01$, ***$p < 0.001$, ****$p < 0.0001$. HFD, high-fat diet; NFD, normal-fat diet; LG, lacrimal gland; MG meibomian gland; w, weeks.

pro-inflammatory responses, adipogenesis, apoptosis, and autophagy in human MG epithelial cells, suggesting a potential protective role of MLT in MGD.[36]

However, the effects and mechanisms of MLT on MGs and LGs remain unclear. This study aimed to investigate the therapeutic effects and mechanisms of action of MLT on high-fat-diet-induced dry eye disease in mice. To the best of our knowledge, this is the first study to validate the effect of MLT on the OSM in an animal model and to drive its translational application to clinical practice.

RESULTS

High-fat diet -induced establishment of a mouse model of dry eye disease

After 4 months of HFD feeding, the mice showed significant changes in body size and weight (Figures 1A and 1B), and the serum total cholesterol level increased (Figure 1C), compared with that of their age-matched counterparts after normal-fat diet (NFD) feeding. The MGs and LGs showed significant lipid infiltration (Figures 1D and 1E), suggesting that HFD is an effective method for modeling hyperlipidemia. MG dropout and opening obstruction are important signs of MGD.[37] The degree of MG opening obstruction in mice progressively worsened as the duration of HFD feeding increased (Figure 1F). After 4 months of HFD feeding, the lid margins showed marked depigmentation (Figure 1G). Moreover, the meibum of hyperlipidemic mice appeared milk-like and thick in texture (Figure 1H). A significant decrease in tear secretion was observed after 8 weeks of HFD feeding (Figure 1I), indicating that LG function was damaged at this time. The TBUT decreased after 16 weeks of HFD administration (Figure 1J), indicating a reduction in tear stability. These results suggest that the high-fat diet intervention successfully established a mouse model of dry eye disease.

Melatonin alleviates dry eye signs of hyperlipidemic mice

When MLT concentrations of $\geq 10^{-5}$M were administered, the mice showed an improvement in the blockage of the MG opening, compared with that of the HFD group (Figure 2A). Similarly, MLT concentrations of $\geq 10^{-5}$M increased tear production (Figure 2B) and enhanced tear film stability (Figure 2C). Hematoxylin and eosin staining revealed a large infiltration of inflammatory cells around the MG and LG follicles of hyperlipidemic mice (Figures 2D and 2F), and the inflammatory cells were markedly reduced after 4 weeks of MLT treatment. MLT also reversed the dilatation of MG ducts in hyperlipidemic mice (Figure 2E). Similarly, we found that hyperlipidemia increased lipid deposition in the LGs of mice; however, MLT administration was ineffective in this situation (Figure 2G). These findings suggest that MLT may have an effect on high-fat-diet-induced dry eye disease.

Melatonin attenuates high-fat diet-induced inflammation of the ocular surface microenvironment

Considering that inflammatory factors play an important role in dry eye disease, we first tested the changes in inflammation-related indicators.[38] mRNA was extracted from MGs and reverse-transcribed for RT-qPCR. Primer sequences are shown in Table 1. MLT effectively reduced the upregulation of inflammatory factors caused by hyperlipidemia (Figures 3A–3C). Immunofluorescence staining was performed on MG and LG sections. Hyperlipidemia caused significant upregulation of IL-1β, IL-6, and TNF-α in tissue, and MLT diminished the expression of these inflammatory factors (Figures 3D–3F). F4/80 is a marker of macrophages. We observed that MLT reversed the macrophage aggregation between vesicles caused by hyperlipidemia in MGs. However, MLT did not appear to have such a positive effect on the LGs (Figure 3G). DHE staining allowed for the observation of intracellular ROS. MLT also reduced oxidative stress in the MGs and LGs (Figure 3H). These results suggest that the effect of MLT on the progression of dry eye disease may be related to the inhibition of inflammatory factor release.

IFT27 levels were increased after melatonin administration

To further clarify the molecular mechanisms that regulate dry eye, we used drug sequencing to set up MLT intervention experiments with different concentrations and to detect mRNA expression. We used a short time-series expression miner (STEM) to analyze the differences in the cellular expression of genes between LPS-induced RAW 264.7 cells with or without MLT administration (Figure 4). The heatmap of gene expression between the groups is shown in Figure 5A. As a significant therapeutic effect was observed in the MLT10^{-3}M group, we further investigated the results of the volcano plot of the MLT10^{-3}M group, which showed a significant up-regulation of IFT27. The KEGG results showed that intermolecular interactions played an important role in this process. To investigate the relationship between MLT and IFT27, we further analyzed the fit of the molecules using the docking model, for example, the vina score was −7 and the cavity size was 1839 (Figures 5B–5E). Finally, we examined IFT27 expression in animal experiments, and the results showed that IFT27 expression was significantly increased with MLT concentrations of 10^{-3}M and 10^{-4}M compared with that in the HFD group, with concentration gradients set in a

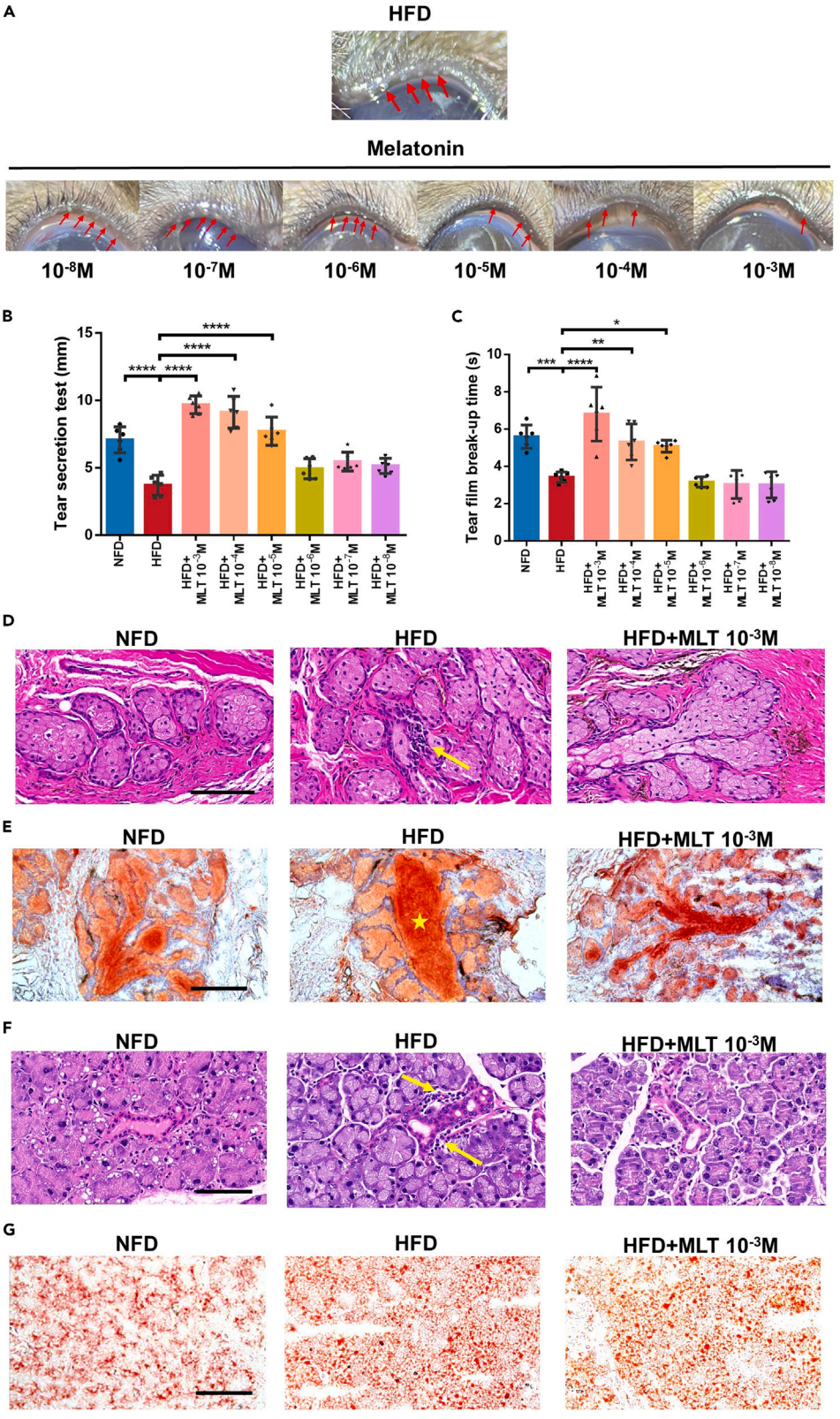
A
HFD
Melatonin
10-8M
10-7M
10-6M
10-5M
10-4M
10-3M
B
Tear secretion test (mm)
C
Tear film break-up time (s)
NFD
HFD
HFD+ MLT 10-3M
HFD+ MLT 10-4M
HFD+ MLT 10-5M
HFD+ MLT 10-6M
HFD+ MLT 10-7M
HFD+ MLT 10-8M
D
NFD
HFD
HFD+MLT 10-3M
E
NFD
HFD
HFD+MLT 10-3M
F
NFD
HFD
HFD+MLT 10-3M
G
NFD
HFD
HFD+MLT 10-3M

Figure 2. MLT alleviated dry eye signs of hyperlipidaemic mice

Representative slit-lamp images showed MLT alleviates the obstruction of MGs openings (red arrows) in HFD mice after 4 weeks of treatment (A). MLT at concentrations above 10^{-5}M improved tear secretion (B) and tear film rupture time (C). Representative hematoxylin and eosin staining exhibited MLT relieved the aggregation of inflammatory cells (yellow arrows) in the MG (D) and LG (F) induced by HFD. Oil Red O staining showed lipid deposition in LG (G), and MLT attenuated lipid deposition and duct dilation (yellow star) in MG (E). Data are shown as mean ± SD; $n = 6$ per group. A one-way ANOVA test was used for statistical analysis. *$p < 0.05$, **$p < 0.01$, ***$p < 0.001$, ****$p < 0.0001$. Scale bars: 100 μm (D, F), 200 μm (E, G). HFD, high-fat diet; NFD, normal-fat diet; LG, lacrimal gland; MG meibomian gland; MLT, melatonin.

concentration-dependent manner (Figures 5F and 5G). These results suggest that IFT27 was significantly up-regulated in the eyelid gland tissues after MLT treatment.

Melatonin decreased M1 macrophages and increased M2 macrophages in dry-eye mice

To investigate the effect of MLT on macrophage regulation in the MG tissues of dry eye disease, we used western blotting (WB) and immunofluorescence to detect the expression of M1 and M2 macrophage-related genes, such as TNF-α, iNOS, CD206, and Arg-1 in the MG tissues. Expression of iNOS and TNF-α was significantly increased in mice undergoing HFD treatment; however, this trend reversed after the use of MLT (Figures 6A–6C). Notably, with MLT 10^{-4} M intervention relative to MLT 10^{-3} M, there was a significant increase in TNF-α levels. Meanwhile, high-fat-diet intervention significantly increased the expression of CD86, and decreased the expression of CD206 and Arg-1, and; intervention with MLT 10^{-3}M further reversed this trend. However, intervention with MLT10^{-4} M decreased the expression of CD206 (Figure 6E). These data suggest that MLT intervention reduces dry eye progression by decreasing lid pro-inflammatory M1 macrophages and increasing anti-inflammatory M2 macrophages.

Knockdown of IFT27 activates the lipopolysaccharide-induced polarization of M1 macrophages in an *in vitro* assay

To further validate that MLT can inhibit M1 macrophage polarization via IFT27, we compared lentivirally transfected macrophages from IFT27, with control lentiviral vectors, and then stimulated them with LPS. WB confirmed the efficiency of the transfection, and LPS stimulation resulted in the macrophage M1-type polarization and induction of pro-inflammatory cytokines such as IL-1β, TNF-α, IL-6, and iNOS expression (Figure 7 A–D). In our study, the knockdown of IFT27 was found to increase LPS-induced inflammatory cytokine production. The results of WB also suggested that the inhibition of IFT27 expression significantly increased the protein levels of iNOS and TNF-α (Figure 7E). Meanwhile, the inhibition of IFT27 significantly increased JNK and ERK phosphorylation (Figure 7E). These data suggest that IFT27 knockdown may activate M1 macrophage polarization.

Knockdown of IFT27 inhibits the interleukin-4-induced polarization of M2 macrophages in an *in vitro* assay

To investigate the effect of MLT on macrophage M2 polarization via IFT27, we first transfected RAW 264.7 cells with lentivirus expressing IFT27 to inhibit the expression of IFT27, and then induced macrophages to reach M2 polarization with 20 ng/mL IL-4. RT-qPCR analysis similarly showed that the knockdown of IFT27 in macrophages inhibited IL-4-induced expression of CD206 and IL-10 (Figures 8A and 8B). These data suggest that knockdown of IFT27 decreased macrophage sensitivity to IL-4, which in turn inhibited M2 macrophage polarization.

Extracellular signal-regulated kinase 1 and c-Jun N-terminal kinase are also involved in the regulation of dry eye disease by melatonin

Digital RNA with the perturbation of genes sequencing (DRUG-seq) was performed to investigate the potential anti-inflammatory and anti-apoptotic effects of MLT. Following Kyoto Encyclopedia of Genes and Genomes (KEGG), gene ontology (GO), Reactome (REAC), and WikiPathways (WP), we found that differential genes were enriched in pathways including the JNK and ERK signaling pathways for each cluster (Figure 4). Immunofluorescence results suggest that MLT intervention significantly inhibited high-fat-diet-induced ERK and JNK phosphorylation (Figure 8C). For validation, we performed protein assays in mouse MGs and found that HFD led to an increase in ERK and JNK phosphorylation, whereas MLT decreased this indicator (Figures 8D and 8E). SENI, which was demonstrated to be an activator of ERK, and ANI, which was an activator of JNK, were used to further validate the role of MLT in the regulation of ERK and JNK phosphorylation. The results suggest that SENI and ANI upregulated ERK and JNK phosphorylation, which was suppressed by MLT. Moreover, after ERK/JNK agonist pretreatment, MLT's negative regulation of inflammatory factors was reversed (Figures S2B and S2C). MLT's up-regulation of IL-4 (a promoter for M2 macrophage polarization) was also diminished by ERK/JNK activation (Figure S2A).

DISCUSSION

In this study, we confirmed the existence of an association between hyperlipidemia and MG/LG dysfunction. We identified the therapeutic effect of MLT eye drops on dry eye disease and further determined that the effect was achieved by regulating macrophage polarization via IFT27 and reducing ERK/JNK phosphorylation.

Patients with hyperlipidemia are more likely to experience dry eyes,[39–41] and MGD, the main cause of evaporative dry eye, is more closely related to hyperlipidemia.[42] Both ApoE-knockout mice and HFD-fed mice can exhibit hypercholesterolemia. ApoE knockout mice exhibited MGD phenotypes, including MG shedding, ductal dilatation, and orifice occlusion, and abnormal MG follicle

Table 1. RT-qPCR primers

Gene	Forward (5′-3′)	Reverse (3′-5′)
β-Actin	GGCTGTATTCCCCTCCATCG	CCAGTTGGTAACAATGCCATGT
TNF-α	CCCTCACACTCAGATCATCTTCT	GCTACGACGTGGGCTACAG
IL-1β	GCAACTGTTCCTGAACTCAACT	ATCTTTTGGGGTCCGTCAACT
IFN-γ	ATGAACGCTACACACTGCATC	CCATCCTTTTGCCAGTTCCTC
IL-4	GGTCTCAACCCCCAGCTAGT	GCCGATGATCTCTCTCAAGTGAT
IFT27	CTGGTGCAGATGTTCCGCA	GTGTCAAGAACTGGCACTGTC
iNOS	GTTCTCAGCCCAACAATACAAGA	GTGGACGGGTCGATGTCAC
CD206	CTCTGTTCAGCTATTGGACGC	CGGAATTTCTGGGATTCAGCTTC
Arg-1	CTCCAAGCCAAAGTCCTTAGAG	AGGAGCTGTCATTAGGGACATC
CD86	TGTTTCCGTGGAGACGCAAG	TTGAGCCTTTGTAAATGGGCA

IFN, interferon; IL, interleukin; TNF, tumor necrosis factor; IFT, intraflagellar transport; iNOS, inducible nitric oxide synthase; Arg, arginase.

morphology.[43] HFD-fed mice exhibited an increased MG area and a greater variety of saturated lipids.[23] Both mice models exhibited inflammation in the MGs and the surrounding environment, as evidenced by the infiltration of inflammatory cells and factors. Inflammation may contribute further to apoptosis of MG cells.[43–45] This finding is comparable to those in our experimental results. HFD caused immune cell infiltration of the LG and increased levels of gene expression of inflammation-related cytokines.[17] This relationship may prevent tear production by destroying alveolar cells and blocking the ducts. However, whether inflammation in the OSM is a primary or subsequent reaction to systemic inflammation caused by an HFD remains unclear. Nevertheless, inflammation is clearly the main trigger of dry eye.

Macrophages are key cells of the innate immune system. Classically activated M1 cells are involved in the initiation and maintenance of inflammation, whereas alternatively activated M2 cells are associated with the abrogation of inflammation.[46] Inflammation linked to an HFD is marked by the accumulation of macrophages in tissues such as fat, liver, or muscle which leads to an increase in pro-inflammatory cytokines.[47] In our study, we found that macrophages with increased M1 polarization and decreased M2 polarization are usually observed in the meibomian glands of mice with dry eye disease, and that an imbalance between M1 and M2 is associated with disease progression. Injection of ex vivo-derived M2 macrophages significantly reduced the progression of ophthalmopathy in mice.[48,49] Similarly, the effective modulation of macrophage polarization *in vivo* may be an effective strategy against retinal degeneration.[50] In this study, we also observed that cytokines were converted from M1-associated cytokines to M2-associated cytokines after MLT treatment.

We found that MLT inhibited the LPS-induced pro-inflammatory cytokine response in RAW 264.7 cells and promoted the secretion of anti-inflammatory factors. MLT affects macrophage function by impacting macrophage development,[51] and modulating macrophage polarization. Notably, MLT affects the macrophage phenotype by reducing M1 macrophage function and promoting M2 macrophage function.[52] MLT plays a key anti-inflammatory role in diabetic wound healing by increasing the M2/M1 ratio and promoting a faster transition from the inflammatory phase to the tissue regeneration phase.[53] Furthermore, MLT can enhance TET-mediated DNA demethylation and raise the M2/M1 ratio via transferring exosomal αKG to macrophages, which alleviates adipocyte inflammation.[54] Therefore, MLT may be used for the prevention and treatment of obesity-induced systemic inflammatory diseases.[54] In addition, MLT exhibits potent antioxidative effects. Excess ROS produced by oxidation leads to inflammatory tissue damage and activates the expression of inflammatory cytokines.[55] In our study, hyperlipidemic mice exhibited increased levels of ROS in MG and LG tissues, which may be associated with lipid deposition in the alveoli.[56,57] In contrast, oxidative stress activates inflammation, which in turn induces the apoptosis of alveolar cells,[58,59] resulting in OSM dysfunction. However, MLT activated antioxidative stress and increased anti-apoptotic protein. MLT is a potent endogenous ROS scavenger.[60] MLT can reduce excess ROS production and maintain mitochondrial function.[61] Intraperitoneal injection of MLT protects the corneal[61] and retinal pigment epithelial cells.[58] Therefore, we hypothesized that MLT reduces inflammation in OSM caused by high lipid levels by modulating macrophage polarization and scavenging excess ROS.

STEM analysis of the sequencing results showed that the differential genes were enriched in the MAPK cascade. Notably, IFT27 also increased significantly after treatment with MLT. IFT27, encoding a small GTPase component of IFT particles, is mutated in a consanguineous family with Bardet-Biedl syndrome.[62] IFT particles are composed of more than 20 unique proteins in 2 subcomplexes called IFT-A and IFT-B.[63] IFT particles are thought to serve as cargo adapters that connect proteins needed to build cilia to molecular motors so that ciliary structural components can be assembled from the cell body into the cilium.[64,65] The IFT27 knockout mice exhibited weakened hedgehog signaling and dysfunctional hedgehog signaling was observed in both the embryo and in fibroblasts derived from the animals.[66] In the present study, we analyzed the relationship between IFT27 and macrophage polarization for the first time, and provided crucial insights for the future regulation of macrophage polarization through the modulation of IFT27 to improve the progression of dry eye disease.

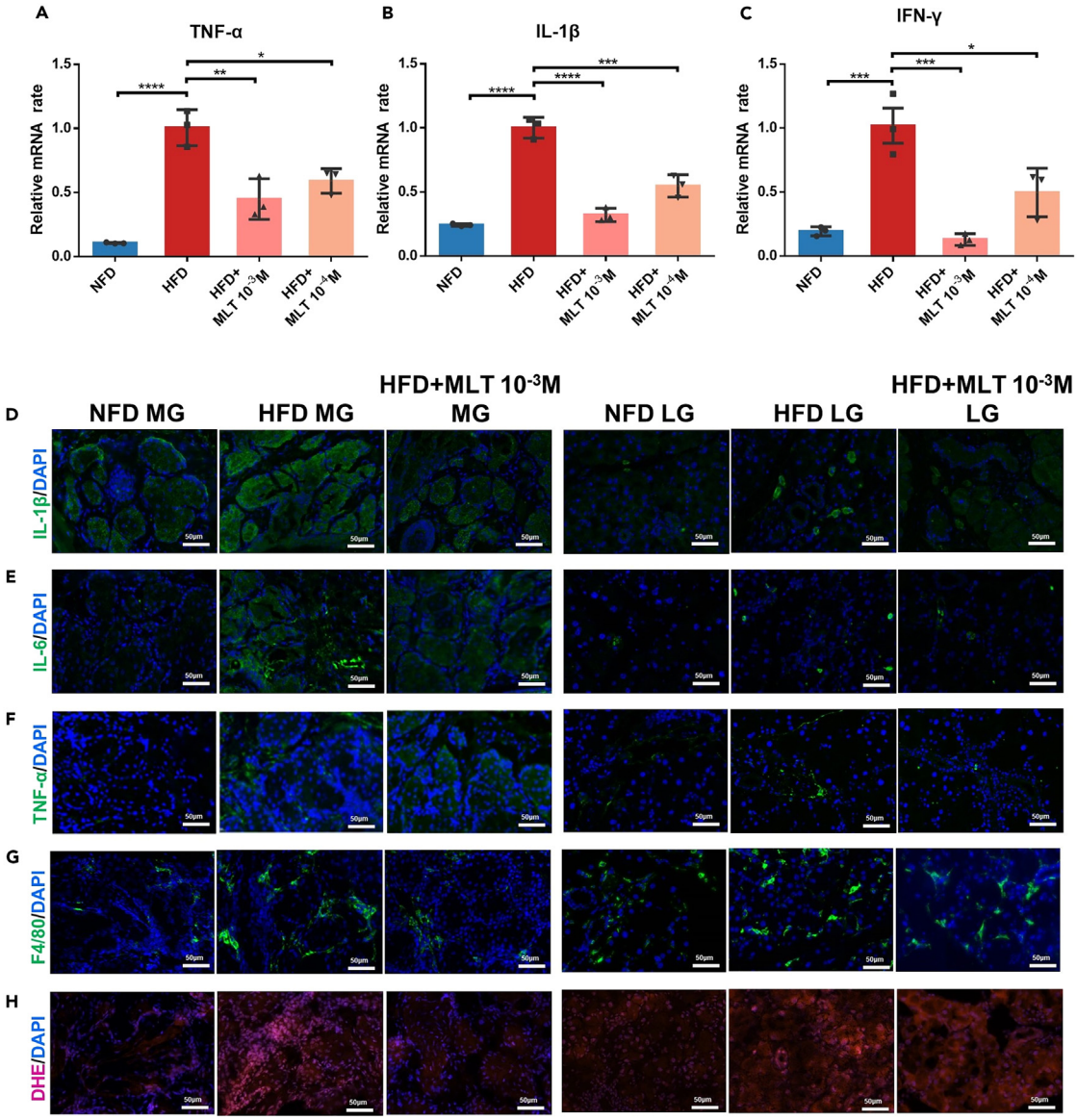

Figure 3. MLT attenuated HFD-induced inflammation of the ocular surface microenvironment

mRNA levels of TNF-α (A), IL-1β (B), and IFN-γ (C) disclosed significant downregulation in MGs after MLT treatment compared to HFD mice. MLT decreased IL-1β (D), IL-6 (E), and TNF-α (F) immunofluorescence staining in both MG and LG of HFD mice. F4/80 positive cells characterized macrophages in MG and LG (G). MLT reduced reactive oxygen species levels in MG and LG detected by dihydroethidium staining (H). Data are shown as mean ± SD; $n = 3$ per group. A one-way ANOVA test was used for statistical analysis. *$p < 0.05$, **$p < 0.01$, ***$p < 0.001$, ****$p < 0.0001$. Scale bars: 50 μm. HFD, high-fat diet; NFD, normal-fat diet; LG, lacrimal gland; MG meibomian gland; MLT, melatonin; TNF, tumor necrosis factor; IL, interleukin; IFN, interferon.

The ERK pathway is the classical pathway for MAPK signaling. In addition to ERK1/2, there are two further members of the MAPK family, c-Jun N-terminal kinase (JNK) and p38 kinase, which have been reported to play a major role in promoting apoptosis.[67–70] Previous studies have found that the activation of the JNK and ERK pathways regulates IL-8 expression and promotes macrophage recruitment.[71] Furthermore, JNK/P38/ERK phosphorylation in the MAPK signaling pathway affects macrophage apoptosis.[72] Zhou et al. also found that β-Elemene regulated M1-M2 macrophage balance through the ERK/JNK/P38 MAPK signaling pathway.[73] Considering the relationship between ERK and JNK signaling pathways and macrophages, we further investigated the expression of ERK and JNK.[74,75] As the ERK/JNK pathway plays an important role in the regulation of for regulating HFD-induced inflammation,[76] which was also confirmed in our study, we hypothesized that MLT functions on HFD-induced dry eye via ERK/JNK. MLT inhibits chondrocyte apoptosis and attenuates inflammatory responses via the MAPK signaling pathway.[77] The protein expression of p38 MAPK is significantly downregulated in diabetes mellitus after MLT treatment, which ultimately exerts a protective effect on the inner blood-retinal barrier.[78] LPS triggered TLR4-mediated pro-inflammatory cytokine

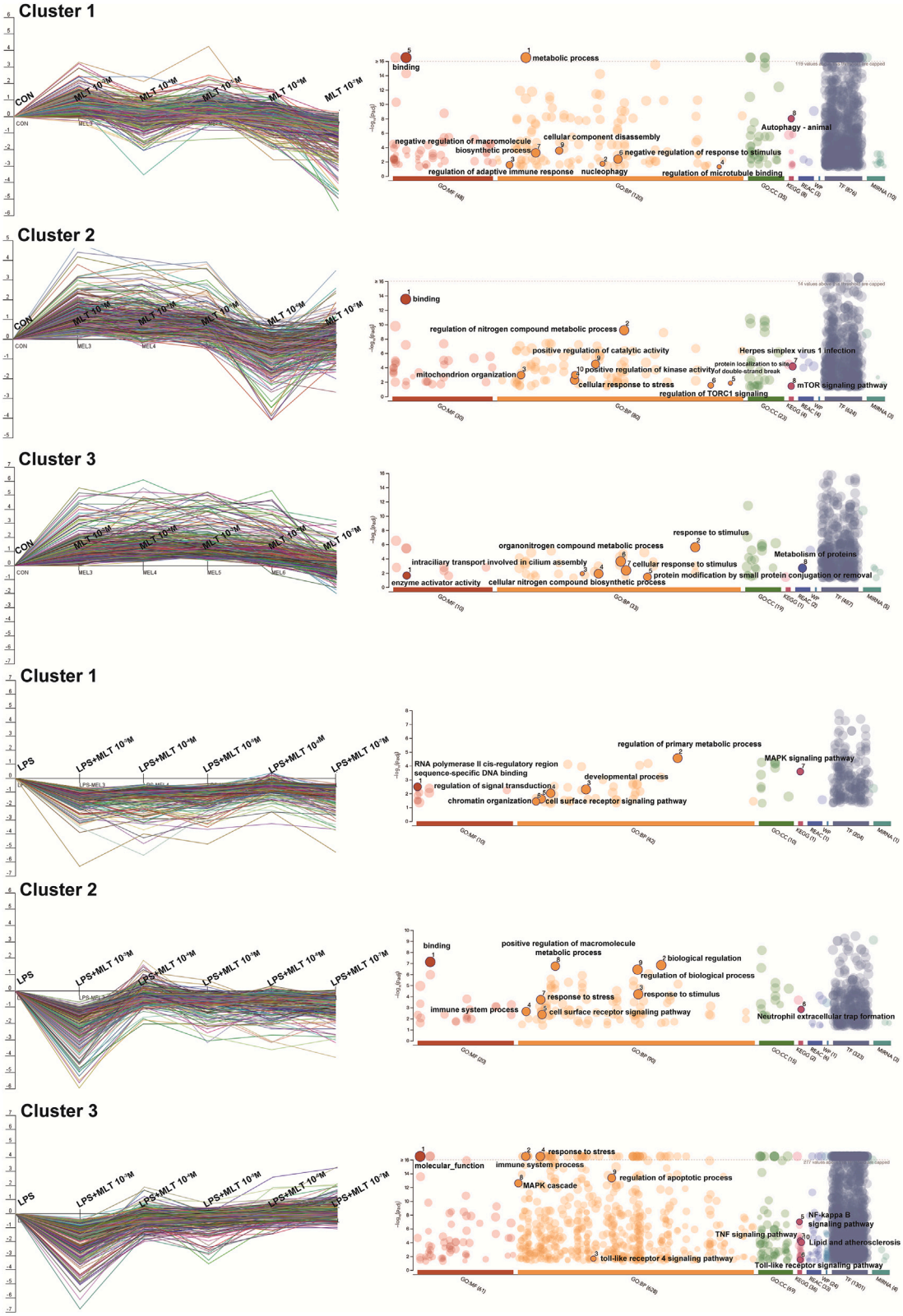
Cluster 1
CON
MLT 10⁻⁹M
MLT 10⁻⁸M
MLT 10⁻⁷M
MLT 10⁻⁶M
MLT 10⁻⁵M
binding
metabolic process
negative regulation of macromolecule biosynthetic process
cellular component disassembly
negative regulation of response to stimulus
regulation of adaptive immune response
nucleophagy
regulation of microtubule binding
Autophagy - animal
Cluster 2
binding
regulation of nitrogen compound metabolic process
positive regulation of catalytic activity
mitochondrion organization
positive regulation of kinase activity
cellular response to stress
regulation of TORC1 signaling
protein localization to site of double-strand break
Herpes simplex virus 1 infection
mTOR signaling pathway
Cluster 3
response to stimulus
organonitrogen compound metabolic process
Metabolism of proteins
intraciliary transport involved in cilium assembly
cellular response to stimulus
protein modification by small protein conjugation or removal
enzyme activator activity
cellular nitrogen compound biosynthetic process
Cluster 1
LPS
LPS+MLT 10⁻⁹M
LPS+MLT 10⁻⁸M
LPS+MLT 10⁻⁷M
LPS+MLT 10⁻⁶M
LPS+MLT 10⁻⁵M
regulation of primary metabolic process
RNA polymerase II cis-regulatory region sequence-specific DNA binding
MAPK signaling pathway
developmental process
regulation of signal transduction
chromatin organization
cell surface receptor signaling pathway
Cluster 2
binding
positive regulation of macromolecule metabolic process
biological regulation
regulation of biological process
response to stress
response to stimulus
immune system process
cell surface receptor signaling pathway
Neutrophil extracellular trap formation
Cluster 3
molecular_function
response to stress
immune system process
regulation of apoptotic process
MAPK cascade
NF-kappa B signaling pathway
TNF signaling pathway
Lipid and atherosclerosis
toll-like receptor 4 signaling pathway
Toll-like receptor signaling pathway

Figure 4. MLT suppressed MAPK pathway according to DRUG-seq

Differential genes were found to be enriched in pathways such as the Toll-like receptor signaling pathway, nuclear factor-κ, and MAPK pathway for each cluster via Kyoto Encyclopedia of Genes and Genomes, Gene Ontology. Reactome, and WikiPathways analysis. DRUG-seq, Digital RNA with the perturbation of genes; MAPK; mitogen-activated protein kinase; MLT, melatonin.

responses and promoted adipogenesis in LPS-stimulated human MG epithelial cells, and MLT pretreatment inhibits the phosphorylation of MAPK/NF-κB components and exerts anti-inflammatory effects.[36] Therefore, MLT treatment for MGD at the cytosolic level is feasible. Comparably, we found that both LPS-treated RAW 264.7 cells and hyperlipidemic mice models demonstrated markedly increased ERK and JNK phosphorylation. Furthermore, MLT downregulated downstream inflammatory cytokines and ROS production in the MGs and LGs by limiting JNK and ERK phosphorylation, maintaining the health and homeostasis of OSM components.

We found that mouse MG cells expressed MT1 and MT2 receptors, and MT2 was abundantly expressed in the cytoplasm of MG cells (Figure S3). Liu et al. found a similar pattern in human MGs.[36] Whether MLT alters pro-inflammatory factor/anti-inflammatory factor production by affecting macrophage polarization or by binding to MT1 and MT2 receptors and generating a signal cascade requires further investigation. We also found that MLT promoted the phagocytosis of Ox-LDL by macrophages (Figure S2D), with the formation of macrophage-derived foam cells. This contrasts with the findings of most previous studies.[36,79,80] This finding may indicate that MLT tends to induce macrophages to differentiate into the M2 type rather than into foam cells. Additionally, the Ox-LDL content between tissues may be reduced because of enhanced phagocytosis by macrophages, although further research is required to clarify this process.

Limitations of the study

This study examined the use of a moderate dose of MLT as therapeutic management for dry eye disease. However, further research is required to determine the optimal drug concentration. IFT27 knockdown in RAW 264.7 cells can impact downstream ERK/JNK

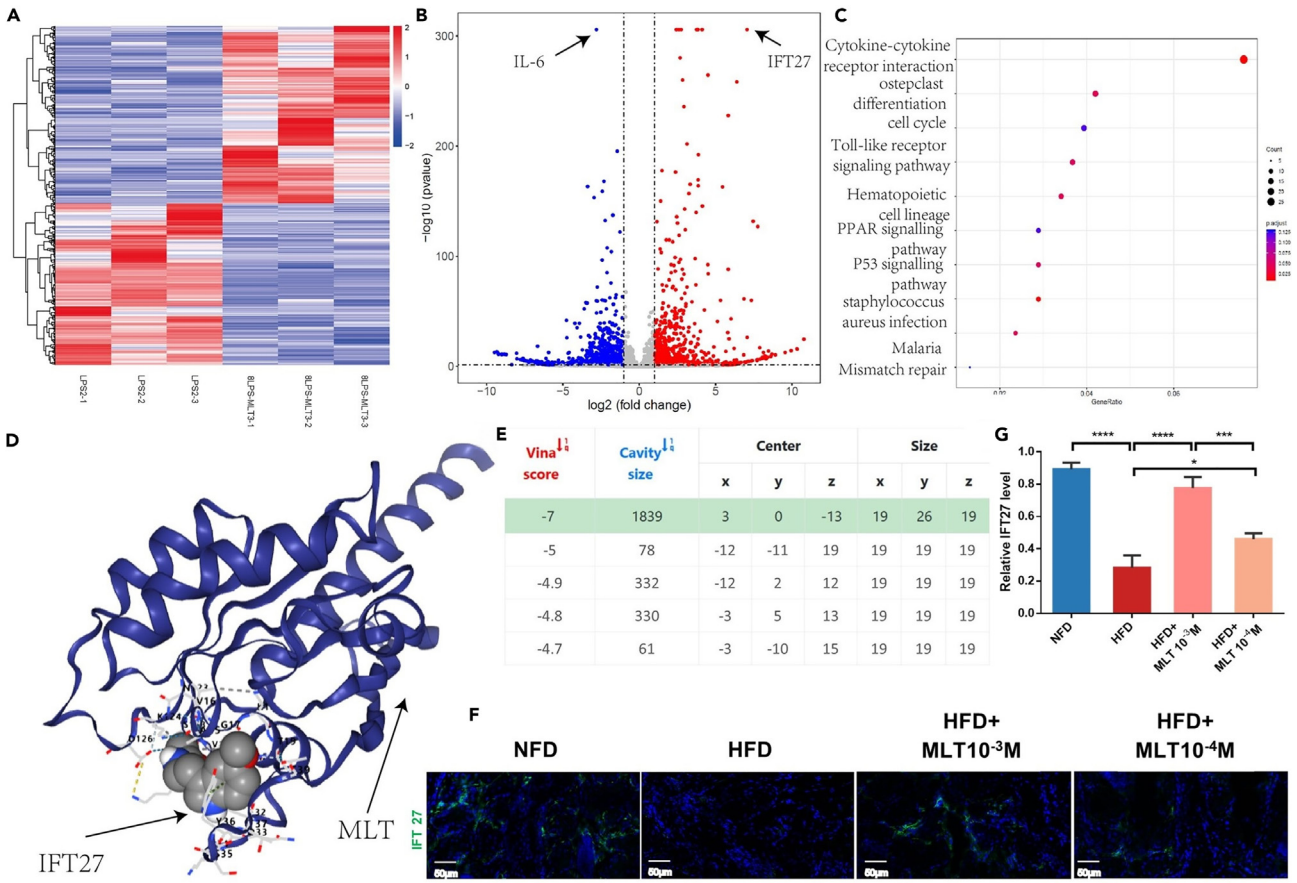

Figure 5. IFT27 binded well to MLT in molecular conformation as a differential gene

(A) heatmap of gene expression among different concentrations of MLT; B, the volcano plot suggested that IFT27 is significantly increased by intervention at MLT10^{-3}M concentrations; C, KEGG pathway; D, Docking model between IFT27 and MLT; E, vina score and cavity size; F, G, The expression of IFT27 in HFD and MLT treatment. Data are shown as mean ± SD; n = 3 per group. A one-way ANOVA test was used for statistical analysis. *p < 0.05, **p < 0.01, ***p < 0.001, ****p < 0.0001. Scale bars: 50 μm. HFD, high-fat diet; NFD, normal-fat diet; MLT, melatonin; IFT, intraflagellar transport.

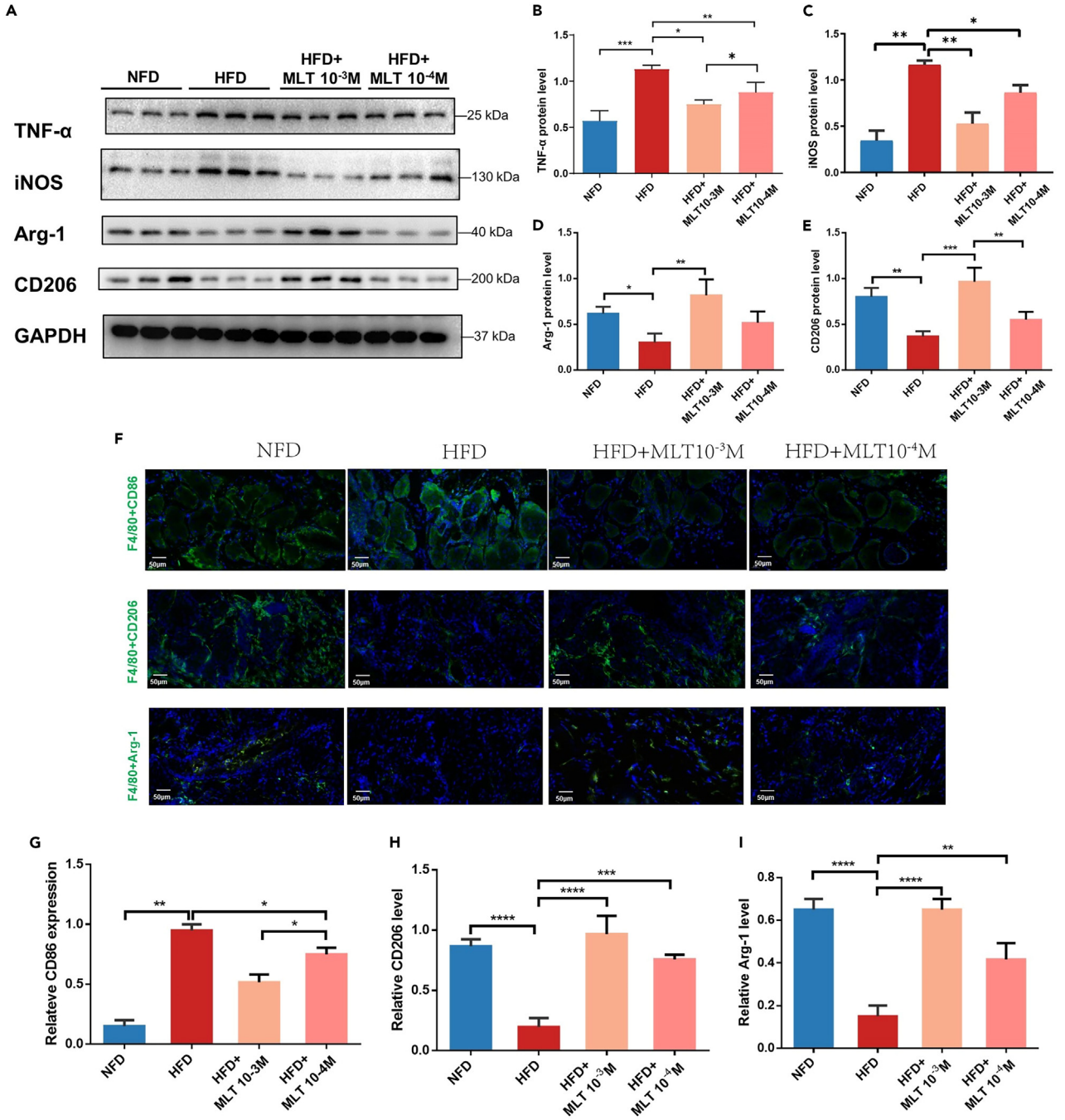

Figure 6. MLT decreased M1 macrophages and increased M2 macrophages in dry eye mice

(A–E) Western blot showed TNF-α, iNOS, Arg-1 and CD206 in meibomian glands after treated with MLT; F-I, Immunofluorescence results showed CD86, CD206 and Arg-1 in meibomian glands after treated with MLT. Data are shown as mean ± SD; $n = 3$ per group. A one-way ANOVA test was used for statistical analysis. $^{*}p < 0.05$, $^{**}p < 0.01$, $^{***}p < 0.001$, $^{****}p < 0.0001$. Scale bars: 50 μm. HFD, high-fat diet; NFD, normal-fat diet; MLT, melatonin; TNF, tumor necrosis factor; iNOS, inducible nitric oxide synthase; Arg, arginase.

phosphorylation, although this has not been verified *in vivo*, and the regulatory role of IFT27 on meibomian cells needs to be identified *in vitro*. Furthermore, we clarified that MLT binds to IFT27 reducing ERK/JNK phosphorylation, although the underlying mechanism of action could not be identified. This will be the focus of our future investigations.

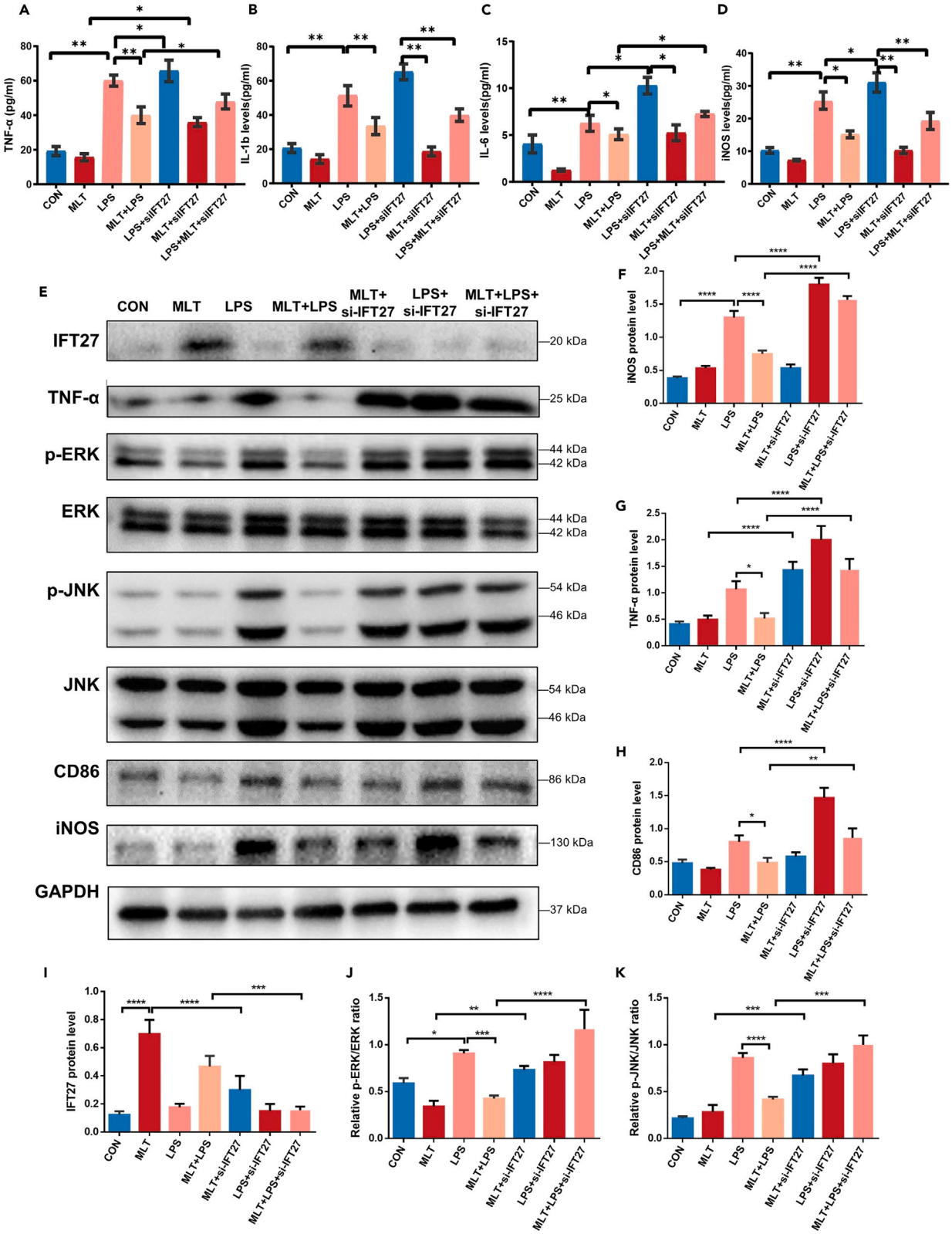
A
TNF-α (pg/ml)
B
IL-1b levels(pg/ml)
C
IL-6 levels(pg/ml)
D
iNOS levels(pg/ml)
CON
MLT
LPS
MLT+LPS
LPS+siIFT27
MLT+siIFT27
LPS+MLT+siIFT27
E
CON
MLT
LPS
MLT+LPS
MLT+ si-IFT27
LPS+ si-IFT27
MLT+LPS+ si-IFT27
IFT27
TNF-α
p-ERK
ERK
p-JNK
JNK
CD86
iNOS
GAPDH
20 kDa
25 kDa
44 kDa
42 kDa
54 kDa
46 kDa
86 kDa
130 kDa
37 kDa
F
iNOS protein level
G
TNF-α protein level
H
CD86 protein level
I
IFT27 protein level
J
Relative p-ERK/ERK ratio
K
Relative p-JNK/JNK ratio

Figure 7. Knockdown of IFT27 activated LPS-induced polarization of M1 macrophages in an *in vitro* assay

(A–D) ELISA assay revealed the changes in TNF-α, IL-1β, IL-6 and iNOS levels in macrophage supernatant; E-K, Western blot assay showed si-IFT27 treatment activated LPS-induced polarization of M1 macrophages; Data are shown as mean ± SD; $n = 3$ per group. A one-way ANOVA test was used for statistical analysis. *$p < 0.05$, **$p < 0.01$, ***$p < 0.001$, ****$p < 0.0001$. Scale bars: 50 μm. MLT, melatonin; LPS, lipopolysaccharide; IFT, intraflagellar transport; TNF, tumor necrosis factor; iNOS, inducible nitric oxide synthase; IL, interleukin; ERK, extracellular signal-regulated kinase; JNK, Jun N-terminal kinase.

STAR★METHODS

Detailed methods are provided in the online version of this paper and include the following:

- KEY RESOURCES TABLE
- RESOURCE AVAILABILITY
  - Lead contact
  - Materials availability
  - Data and code availability
- EXPERIMENTAL MODEL AND STUDY PARTICIPANT DETAILS
  - Animals and treatment
  - Cell culture and treatment

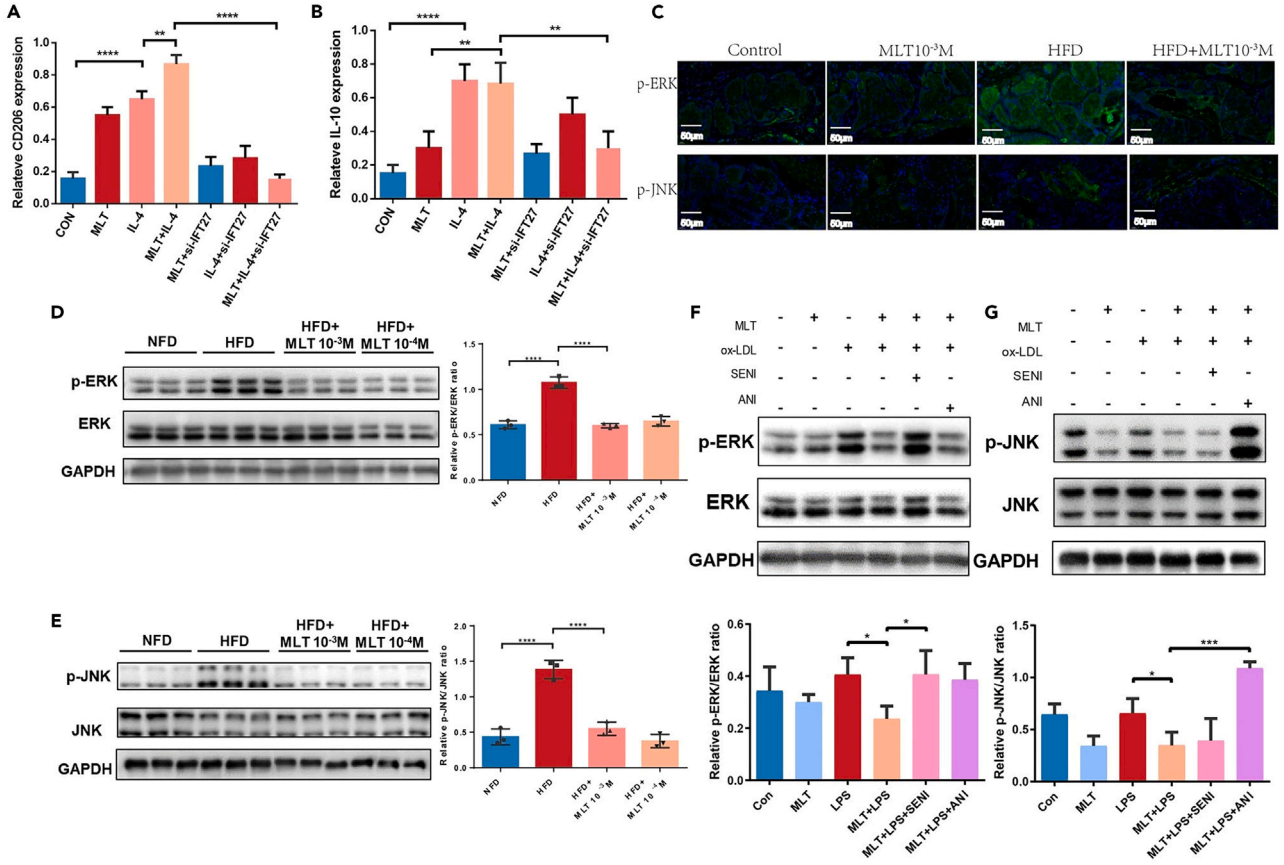

Figure 8. Knockdown of IFT27 inhibited IL-4-induced polarization of M2 macrophages and MLT relieved macrophage inflammation by downregulating JNK/ERK phosphorylation

Knockdown of IFT27 inhibited IL-4-induced polarization of M2 macrophages (A and B). Immunofluorescence results showed phosphorylated ERK and JNK expression after treated with MLT (C). Western blot analysis showed a decrease in the phosphorylation of ERK/JNK in MGs after MLT treatment (D and E). *In vitro*, protein bands showed that the inhibitory effect of MLT on ERK/JNK phosphorylation can be activated by SENI and ANI (F and G). Data are shown as mean ± SD; $n = 3$ per group. A one-way ANOVA test was used for statistical analysis. *$p < 0.05$, ***$p < 0.001$, ****$p < 0.0001$. IL, interleukin; ERK, extracellular signal-regulated kinases; JNK, -Jun N-terminal kinase; LPS, lipopolysaccharide; IFT, intraflagellar transport; MLT, melatonin; ANI, anisomycin; SENI, senkyunolide I.

SUPPLEMENTAL INFORMATION

Supplemental information can be found online at https://doi.org/10.1016/j.isci.2024.110367.

ACKNOWLEDGMENTS

This study was supported by the National Natural Science Foundation of China (No.82271050), the Youth Program of National Natural Science Foundation of China (No.82301175), the Yangfan Plan of Shanghai Science and Technology Commission (No.22YF1443100), and the Project of Key Disciplines of Medicine in Yangpu District of Shanghai (No.22YPZA01).

AUTHOR CONTRIBUTIONS

CYY: Conceptualization, investigation, data curation, and writing. ZX: Conceptualization, formal analysis, and methodology. YCX: Review and editing. JYP: Conceptualization and funding acquisition. CYH: Formal analysis and funding acquisition. All authors approved the final version of the article.

DECLARATION OF INTERESTS

The authors declare no competing interests.

Received: January 11, 2024
Revised: March 3, 2024
Accepted: June 21, 2024
Published: June 24, 2024

REFERENCES

1. Hakim, F.E., and Farooq, A.V. (2022). Dry Eye Disease: An Update in 2022. JAMA *327*, 478–479. https://doi.org/10.1001/jama.2021.19963.
2. Mittal, R., Patel, S., and Galor, A. (2021). Alternative therapies for dry eye disease. Curr. Opin. Ophthalmol. *32*, 348–361. https://doi.org/10.1097/icu.0000000000000768.
3. Zhang, X., Jeyalatha, M.V., Qu, Y., He, X., Ou, S., Bu, J., Jia, C., Wang, J., Wu, H., Liu, Z., and Li, W. (2017). Dry Eye Management: Targeting the Ocular Surface Microenvironment. Int. J. Mol. Sci. *18*, 1398. https://doi.org/10.3390/ijms18071398.
4. Willcox, M.D.P., Argüeso, P., Georgiev, G.A., Holopainen, J.M., Laurie, G.W., Millar, T.J., Papas, E.B., Rolland, J.P., Schmidt, T.A., Stahl, U., et al. (2017). TFOS DEWS II Tear Film Report. Ocul. Surf. *15*, 366–403. https://doi.org/10.1016/j.jtos.2017.03.006.
5. Tsai, P.S., Evans, J.E., Green, K.M., Sullivan, R.M., Schaumberg, D.A., Richards, S.M., Dana, M.R., and Sullivan, D.A. (2006). Proteomic analysis of human meibomian gland secretions. Br. J. Ophthalmol. *90*, 372–377. https://doi.org/10.1136/bjo.2005.080846.
6. Conrady, C.D., Joos, Z.P., and Patel, B.C.K. (2016). Review: The Lacrimal Gland and Its Role in Dry Eye. J. Ophthalmol. *2016*, 7542929. https://doi.org/10.1155/2016/7542929.
7. Lemp, M.A., and Foulks, G.N. (2007). The definition and classification of dry eye disease: report of the Definition and Classification Subcommittee of the International Dry Eye WorkShop. Ocul. Surf. *5*, 75–92. https://doi.org/10.1016/s1542-0124(12)70081-2.
8. Chan, T.C.Y., Chow, S.S.W., Wan, K.H.N., and Yuen, H.K.L. (2019). Update on the association between dry eye disease and meibomian gland dysfunction. Hong Kong Med. J. *25*, 38–47. https://doi.org/10.12809/hkmj187331.
9. Walter, K. (2022). What Is Dry Eye Disease? JAMA *328*, 84. https://doi.org/10.1001/jama.2022.5978.
10. Dao, A.H., Spindle, J.D., Harp, B.A., Jacob, A., Chuang, A.Z., and Yee, R.W. (2010). Association of dyslipidemia in moderate to severe meibomian gland dysfunction. Am. J. Ophthalmol. *150*, 371–375.e1. https://doi.org/10.1016/j.ajo.2010.04.016.
11. Pinna, A., Blasetti, F., Zinellu, A., Carru, C., and Solinas, G. (2013). Meibomian gland dysfunction and hypercholesterolemia. Ophthalmology *120*, 2385–2389. https://doi.org/10.1016/j.ophtha.2013.05.002.
12. Bukhari, A.A. (2013). Associations between the grade of meibomian gland dysfunction and dyslipidemia. Ophthalmic Plast. Reconstr. Surg. *29*, 101–103. https://doi.org/10.1097/IOP.0b013e31827a007d.
13. Kuriakose, R.K., and Braich, P.S. (2018). Dyslipidemia and its Association with Meibomian Gland Dysfunction: A Systematic Review. Int. Ophthalmol. *38*, 1809–1816. https://doi.org/10.1007/s10792-017-0633-0.
14. Boulangé, C.L., Neves, A.L., Chilloux, J., Nicholson, J.K., and Dumas, M.E. (2016). Impact of the gut microbiota on inflammation, obesity, and metabolic disease. Genome Med. *8*, 42. https://doi.org/10.1186/s13073-016-0303-2.

15. Dettmer, R., Niwolik, I., Cirksena, K., Yoshimoto, T., Tang, Y., Mehmeti, I., Gurgul-Convey, E., and Naujok, O. (2022). Proinflammatory cytokines induce rapid, NO-independent apoptosis, expression of chemotactic mediators and interleukin-32 secretion in human pluripotent stem cell-derived beta cells. Diabetologia *65*, 829–843. https://doi.org/10.1007/s00125-022-05654-0.
16. Liao, M.F., Lu, K.T., Hsu, J.L., Lee, C.H., Cheng, M.Y., and Ro, L.S. (2022). The Role of Autophagy and Apoptosis in Neuropathic Pain Formation. Int. J. Mol. Sci. *23*, 2685. https://doi.org/10.3390/ijms23052685.
17. He, X., Zhao, Z., Wang, S., Kang, J., Zhang, M., Bu, J., Cai, X., Jia, C., Li, Y., Li, K., et al. (2020). High-Fat Diet-Induced Functional and Pathologic Changes in Lacrimal Gland. Am. J. Pathol. *190*, 2387–2402. https://doi.org/10.1016/j.ajpath.2020.09.002.
18. Perez, V.L., Stern, M.E., and Pflugfelder, S.C. (2020). Inflammatory basis for dry eye disease flares. Exp. Eye Res. *201*, 108294. https://doi.org/10.1016/j.exer.2020.108294.
19. Perez, V.L., Mah, F.S., Willcox, M., and Pflugfelder, S. (2023). Anti-Inflammatories in the Treatment of Dry Eye Disease: A Review. J. Ocul. Pharmacol. Therapeut. *39*, 89–101. https://doi.org/10.1089/jop.2022.0133.
20. Nair, A.P., D'Souza, S., Khamar, P., Nuijts, R.M.M.A., Sethu, S., and Shetty, R. (2023). Ocular surface immune cell diversity in dry eye disease. Indian J. Ophthalmol. *71*, 1237–1247. https://doi.org/10.4103/ijo.Ijo_2986_22.
21. Yunna, C., Mengru, H., Lei, W., and Weidong, C. (2020). Macrophage M1/M2 polarization. Eur. J. Pharmacol. *877*, 173090. https://doi.org/10.1016/j.ejphar.2020.173090.
22. Shapouri-Moghaddam, A., Mohammadian, S., Vazini, H., Taghadosi, M., Esmaeili, S.A., Mardani, F., Seifi, B., Mohammadi, A., Afshari, J.T., and Sahebkar, A. (2018). Macrophage plasticity, polarization, and function in health and disease. J. Cell. Physiol. *233*, 6425–6440. https://doi.org/10.1002/jcp.26429.
23. Wang, J., Long, R., and Han, Y. (2022). The role of exosomes in the tumour microenvironment on macrophage polarisation. Biochim. Biophys. Acta Rev. Canc *1877*, 188811. https://doi.org/10.1016/j.bbcan.2022.188811.
24. Sun, Y., Liu, W.Z., Liu, T., Feng, X., Yang, N., and Zhou, H.F. (2015). Signaling pathway of MAPK/ERK in cell proliferation, differentiation, migration, senescence and apoptosis. J. Recept. Signal Transduct. Res. *35*, 600–604. https://doi.org/10.3109/10799893.2015.1030412.
25. Rousseau, S., and Martel, G. (2016). Gain-of-Function Mutations in the Toll-Like Receptor Pathway: TPL2-Mediated ERK1/ERK2 MAPK Activation, a Path to Tumorigenesis in Lymphoid Neoplasms? Front. Cell Dev. Biol. *4*, 50. https://doi.org/10.3389/fcell.2016.00050.
26. Ni, L., Zheng, Y., Gong, T., Xiu, C., Li, K., Chen, J., Saijilafu, Li, B., Li, B., and Yang, H. (2019). Proinflammatory macrophages promote degenerative phenotypes in rat nucleus pulpous cells partly through ERK and JNK signaling. J. Cell. Physiol. *234*, 5362–5371. https://doi.org/10.1002/jcp.27507.
27. Xie, X.D., Tang, M., Yi, S.L., He, Y., Chen, S.Y., Zhao, Y., Chen, Q., Cao, M.X., Yu, M.L., Wei, Y.Y., et al. (2024). Polysaccharide of Asparagus cochinchinensis (Lour.) Merr regulates macrophage immune response and epigenetic memory through TLR4-JNK/p38/ERK signaling pathway and histone modification. Phytomedicine *124*, 155294. https://doi.org/10.1016/j.phymed.2023.155294.
28. Zhu, H., Zhang, L., Jia, H., Xu, L., Cao, Y., Zhai, M., Li, K., Xia, L., Jiang, L., Li, X., et al. (2022). Tetrahydrocurcumin improves lipopolysaccharide-induced myocardial dysfunction by inhibiting oxidative stress and inflammation via JNK/ERK signaling pathway regulation. Phytomedicine *104*, 154283. https://doi.org/10.1016/j.phymed.2022.154283.
29. Mantawy, E.M., Said, R.S., and Abdel-Aziz, A.K. (2019). Mechanistic approach of the inhibitory effect of chrysin on inflammatory and apoptotic events implicated in radiation-induced premature ovarian failure: Emphasis on TGF-β/MAPKs signaling pathway. Biomed. Pharmacother. *109*, 293–303. https://doi.org/10.1016/j.biopha.2018.10.092.
30. Wang, M., Crisostomo, P.R., Herring, C., Meldrum, K.K., and Meldrum, D.R. (2006). Human progenitor cells from bone marrow or adipose tissue produce VEGF, HGF, and IGF-I in response to TNF by a p38 MAPK-dependent mechanism. Am. J. Physiol. Regul. Integr. Comp. Physiol. *291*, R880–R884. https://doi.org/10.1152/ajpregu.00280.2006.
31. Montalbano, G., Mania, M., Abbate, F., Navarra, M., Guerrera, M.C., Laura, R., Vega, J.A., Levanti, M., and Germanà, A. (2018). Melatonin treatment suppresses appetite genes and improves adipose tissue plasticity in diet-induced obese zebrafish. Endocrine *62*, 381–393. https://doi.org/10.1007/s12020-018-1653-x.
32. Lardone, P.J., Alvarez-Sanchez, S.N., Guerrero, J.M., and Carrillo-Vico, A. (2014). Melatonin and glucose metabolism: clinical relevance. Curr. Pharmaceut. Des. *20*, 4841–4853. https://doi.org/10.2174/1381612819666131119101032.
33. Xu, P., Wang, J., Hong, F., Wang, S., Jin, X., Xue, T., Jia, L., and Zhai, Y. (2017). Melatonin prevents obesity through modulation of gut microbiota in mice. J. Pineal Res. *62*, e12399. https://doi.org/10.1111/jpi.12399.
34. Jiang, T., Chang, Q., Cai, J., Fan, J., Zhang, X., and Xu, G. (2016). Protective Effects of Melatonin on Retinal Inflammation and Oxidative Stress in Experimental Diabetic Retinopathy. Oxid. Med. Cell. Longev. *2016*, 3528274. https://doi.org/10.1155/2016/3528274.
35. Mi, Y., Wei, C., Sun, L., Liu, H., Zhang, J., Luo, J., Yu, X., He, J., Ge, H., and Liu, P. (2023). Melatonin inhibits ferroptosis and delays age-related cataract by regulating SIRT6/p-Nrf2/GPX4 and SIRT6/NCOA4/FTH1 pathways. Biomed. Pharmacother. *157*, 114048. https://doi.org/10.1016/j.biopha.2022.114048.
36. Liu, R., Li, J., Xu, Y., Chen, Z., Ye, H., Tang, J., Wei, L., and Liang, L. (2022). Melatonin Attenuates LPS-Induced Proinflammatory Cytokine Response and Lipogenesis in Human Meibomian Gland Epithelial Cells via MAPK/NF-κB Pathway. Invest. Ophthalmol. Vis. Sci. *63*, 6. https://doi.org/10.1167/iovs.63.5.6.
37. Yin, Y., and Gong, L. (2017). Reversibility of Gland Dropout and Significance of Eyelid Hygiene Treatment in Meibomian Gland Dysfunction. Cornea *36*, 332–337. https://doi.org/10.1097/ICO.0000000000001042.
38. Han, Y., Guo, S., Li, Y., Li, J., Zhu, L., Liu, Y., Lv, Y., Yu, D., Zheng, L., Huang, C., et al. (2023). Berberine ameliorate inflammation and apoptosis via modulating PI3K/AKT/NFκB and MAPK pathway on dry eye. Phytomedicine *121*, 155081. https://doi.org/10.1016/j.phymed.2023.155081.
39. Rathnakumar, K., Ramachandran, K., Baba, D., Ramesh, V., Anebaracy, V., Vidhya, R., Vinothkumar, R., Poovitha, R., and Geetha, R. (2018). Prevalence of dry eye disease and its association with dyslipidemia. J. Basic Clin. Physiol. Pharmacol. *29*, 195–199. https://doi.org/10.1515/jbcpp-2017-0001.
40. Aldaas, K.M., Ismail, O.M., Hakim, J., Van Buren, E.D., Lin, F.C., Hardin, J.S., and Meyer, J.J. (2020). Association of Dry Eye Disease With Dyslipidemia and Statin Use. Am. J. Ophthalmol. *218*, 54–58. https://doi.org/10.1016/j.ajo.2020.05.007.
41. Chun, Y.H., Kim, H.R., Han, K., Park, Y.G., Song, H.J., and Na, K.S. (2013). Total cholesterol and lipoprotein composition are associated with dry eye disease in Korean women. Lipids Health Dis. *12*, 84. https://doi.org/10.1186/1476-511X-12-84.
42. Tomioka, Y., Kitazawa, K., Yamashita, Y., Numa, K., Inomata, T., Hughes, J.W.B., Soda, R., Nakamura, M., Suzuki, T., Yokoi, N., and Sotozono, C. (2023). Dyslipidemia Exacerbates Meibomian Gland Dysfunction: A Systematic Review and Meta-Analysis. J. Clin. Med. *12*, 2131. https://doi.org/10.3390/jcm12062131.
43. Bu, J., Zhang, M., Wu, Y., Jiang, N., Guo, Y., He, X., He, H., Jeyalatha, M.V., Reinach, P.S., Liu, Z., and Li, W. (2021). High-Fat Diet Induces Inflammation of Meibomian Gland. Invest. Ophthalmol. Vis. Sci. *62*, 13. https://doi.org/10.1167/iovs.62.10.13.
44. Osae, E.A., Bullock, T., Chintapalati, M., Brodesser, S., Hanlon, S., Redfern, R., Steven, P., Smith, C.W., Rumbaut, R.E., and Burns, A.R. (2020). Obese Mice with Dyslipidemia Exhibit Meibomian Gland Hypertrophy and Alterations in Meibum Composition and Aqueous Tear Production. Int. J. Mol. Sci. *21*, 8772. https://doi.org/10.3390/ijms21228772.
45. Bu, J., Wu, Y., Cai, X., Jiang, N., Jeyalatha, M.V., Yu, J., He, X., He, H., Guo, Y., Zhang, M., et al. (2019). Hyperlipidemia induces meibomian gland dysfunction. Ocul. Surf. *17*, 777–786. https://doi.org/10.1016/j.jtos.2019.06.002.
46. Chen, S., Cui, W., Chi, Z., Xiao, Q., Hu, T., Ye, Q., Zhu, K., Yu, W., Wang, Z., Yu, C., et al. (2022). Tumor-associated macrophages are shaped by intratumoral high potassium via Kir2.1. Cell Metabol. *34*, 1843–1859.e11. https://doi.org/10.1016/j.cmet.2022.08.016.
47. Hotamisligil, G.S. (2006). Inflammation and metabolic disorders. Nature *444*, 860–867. https://doi.org/10.1038/nature05485.
48. Lei, A., Yu, H., Lu, S., Lu, H., Ding, X., Tan, T., Zhang, H., Zhu, M., Tian, L., Wang, X., et al. (2024). A second-generation M1-polarized CAR macrophage with antitumor efficacy. Nat. Immunol. *25*, 102–116. https://doi.org/10.1038/s41590-023-01687-8.
49. Peng, Y., Zhou, M., Yang, H., Qu, R., Qiu, Y., Hao, J., Bi, H., and Guo, D. (2023). Regulatory Mechanism of M1/M2 Macrophage Polarization in the Development of Autoimmune Diseases. Mediat. Inflamm. *2023*, 8821610. https://doi.org/10.1155/2023/8821610.
50. Jiao, H., Natoli, R., Valter, K., Provis, J.M., and Rutar, M. (2015). Spatiotemporal Cadence of Macrophage Polarisation in a Model of

Light-Induced Retinal Degeneration. PLoS One *10*, e0143952. https://doi.org/10.1371/journal.pone.0143952.

51. Haldar, C., Häussler, D., and Gupta, D. (1992). Effect of the pineal gland on circadian rhythmicity of colony forming units for granulocytes and macrophages (CFU-GM) from rat bone marrow cell cultures. J. Pineal Res. *12*, 79–83. https://doi.org/10.1111/j.1600-079x.1992.tb00030.x.
52. Xia, Y., Chen, S., Zeng, S., Zhao, Y., Zhu, C., Deng, B., Zhu, G., Yin, Y., Wang, W., Hardeland, R., and Ren, W. (2019). Melatonin in macrophage biology: Current understanding and future perspectives. J. Pineal Res. *66*, e12547. https://doi.org/10.1111/jpi.12547.
53. Liu, W., Yu, M., Xie, D., Wang, L., Ye, C., Zhu, Q., Liu, F., and Yang, L. (2020). Melatonin-stimulated MSC-derived exosomes improve diabetic wound healing through regulating macrophage M1 and M2 polarization by targeting the PTEN/AKT pathway. Stem Cell Res. Ther. *11*, 259. https://doi.org/10.1186/s13287-020-01756-x.
54. Liu, Z., Gan, L., Zhang, T., Ren, Q., and Sun, C. (2018). Melatonin alleviates adipose inflammation through elevating alpha-ketoglutarate and diverting adipose-derived exosomes to macrophages in mice. J. Pineal Res. *64*, e12455. https://doi.org/10.1111/jpi.12455.
55. Mittal, M., Siddiqui, M.R., Tran, K., Reddy, S.P., and Malik, A.B. (2014). Reactive oxygen species in inflammation and tissue injury. Antioxidants Redox Signal. *20*, 1126–1167. https://doi.org/10.1089/ars.2012.5149.
56. Rosa, D.F., Sarandy, M.M., Novaes, R.D., Freitas, M.B., do Carmo Gouveia Pelúzio, M., and Gonçalves, R.V. (2018). High-Fat Diet and Alcohol Intake Promotes Inflammation and Impairs Skin Wound Healing in Wistar Rats. Mediat. Inflamm. *2018*, 4658583. https://doi.org/10.1155/2018/4658583.
57. Airaksinen, K., Jokkala, J., Ahonen, I., Auriola, S., Kolehmainen, M., Hanhineva, K., and Tiihonen, K. (2018). High-Fat Diet, Betaine, and Polydextrose Induce Changes in Adipose Tissue Inflammation and Metabolism in C57BL/6J Mice. Mol. Nutr. Food Res. *62*, e1800455. https://doi.org/10.1002/mnfr.201800455.
58. Chang, C.C., Huang, T.Y., Chen, H.Y., Huang, T.C., Lin, L.C., Chang, Y.J., and Hsia, S.M. (2018). Protective Effect of Melatonin against Oxidative Stress-Induced Apoptosis and Enhanced Autophagy in Human Retinal Pigment Epithelium Cells. Oxid. Med. Cell. Longev. *2018*, 9015765. https://doi.org/10.1155/2018/9015765.
59. Wang, S., Irving, G., Jiang, L., Wang, H., Li, M., Wang, X., Han, W., Xu, Y., Yang, Y., Zeng, T., et al. (2017). Oxidative Stress Mediated Hippocampal Neuron Apoptosis Participated in Carbon Disulfide-Induced Rats Cognitive Dysfunction. Neurochem. Res. *42*, 583–594. https://doi.org/10.1007/s11064-016-2113-8.
60. Tan, D.X., Manchester, L.C., Esteban-Zubero, E., Zhou, Z., and Reiter, R.J. (2015). Melatonin as a Potent and Inducible Endogenous Antioxidant: Synthesis and Metabolism. Molecules *20*, 18886–18906. https://doi.org/10.3390/molecules201018886.
61. Wang, B., Zuo, X., Peng, L., Wang, X., Zeng, H., Zhong, J., Li, S., Xiao, Y., Wang, L., Ouyang, H., and Yuan, J. (2021). Melatonin ameliorates oxidative stress-mediated injuries through induction of HO-1 and restores autophagic flux in dry eye. Exp. Eye Res. *205*, 108491. https://doi.org/10.1016/j.exer.2021.108491.
62. Aldahmesh, M.A., Li, Y., Alhashem, A., Anazi, S., Alkuraya, H., Hashem, M., Awaji, A.A., Sogaty, S., Alkharashi, A., Alzahrani, S., et al. (2014). IFT27, encoding a small GTPase component of IFT particles, is mutated in a consanguineous family with Bardet-Biedl syndrome. Hum. Mol. Genet. *23*, 3307–3315. https://doi.org/10.1093/hmg/ddu044.
63. Rosenbaum, J.L., and Witman, G.B. (2002). Intraflagellar transport. Nat. Rev. Mol. Cell Biol. *3*, 813–825. https://doi.org/10.1038/nrm952.
64. Marion, V., Stutzmann, F., Gérard, M., De Melo, C., Schaefer, E., Claussmann, A., Hellé, S., Delague, V., Souied, E., Barrey, C., et al. (2012). Exome sequencing identifies mutations in LZTFL1, a BBSome and smoothened trafficking regulator, in a family with Bardet–Biedl syndrome with situs inversus and insertional polydactyly. J. Med. Genet. *49*, 317–321. https://doi.org/10.1136/jmedgenet-2012-100737.
65. Seo, S., Zhang, Q., Bugge, K., Breslow, D.K., Searby, C.C., Nachury, M.V., and Sheffield, V.C. (2011). A novel protein LZTFL1 regulates ciliary trafficking of the BBSome and Smoothened. PLoS Genet. *7*, e1002358. https://doi.org/10.1371/journal.pgen.1002358.
66. Eguether, T., San Agustin, J.T., Keady, B.T., Jonassen, J.A., Liang, Y., Francis, R., Tobita, K., Johnson, C.A., Abdelhamed, Z.A., Lo, C.W., and Pazour, G.J. (2014). IFT27 links the BBSome to IFT for maintenance of the ciliary signaling compartment. Dev. Cell *31*, 279–290. https://doi.org/10.1016/j.devcel.2014.09.011.
67. Liu, F., Yang, X., Geng, M., and Huang, M. (2018). Targeting ERK, an Achilles' Heel of the MAPK pathway, in cancer therapy. Acta Pharm. Sin. B *8*, 552–562. https://doi.org/10.1016/j.apsb.2018.01.008.
68. Huang, F., Liu, Q., Xie, S., Xu, J., Huang, B., Wu, Y., and Xia, D. (2016). Cypermethrin Induces Macrophages Death through Cell Cycle Arrest and Oxidative Stress-Mediated JNK/ERK Signaling Regulated Apoptosis. Int. J. Mol. Sci. *17*, 885. https://doi.org/10.3390/ijms17060885.
69. Huang, Y.M., Wu, Y.S., Dang, Y.Y., Xu, Y.M., Ma, K.Y., and Dai, X.Y. (2024). Par3L, a polarity protein, promotes M1 macrophage polarization and aggravates atherosclerosis in mice via p65 and ERK activation. Acta Pharmacol. Sin. *45*, 112–124. https://doi.org/10.1038/s41401-023-01161-z.
70. Monick, M.M., Powers, L.S., Barrett, C.W., Hinde, S., Ashare, A., Groskreutz, D.J., Nyunoya, T., Coleman, M., Spitz, D.R., and Hunninghake, G.W. (2008). Constitutive ERK MAPK activity regulates macrophage ATP production and mitochondrial integrity. J. Immunol. *180*, 7485–7496. https://doi.org/10.4049/jimmunol.180.11.7485.
71. You, Y., Wen, D., Zeng, L., Lu, J., Xiao, X., Chen, Y., Song, H., and Liu, Z. (2022). ALKBH5/MAP3K8 axis regulates PD-L1+ macrophage infiltration and promotes hepatocellular carcinoma progression. Int. J. Biol. Sci. *18*, 5001–5018. https://doi.org/10.7150/ijbs.70149.
72. Fang, S., Sun, S., Cai, H., Zou, X., Wang, S., Hao, X., Wan, X., Tian, J., Li, Z., He, Z., et al. (2021). IRGM/Irgm1 facilitates macrophage apoptosis through ROS generation and MAPK signal transduction: Irgm1(+/-) mice display increases atherosclerotic plaque stability. Theranostics *11*, 9358–9375. https://doi.org/10.7150/thno.62797.
73. Zhou, Y., Takano, T., Li, X., Wang, Y., Wang, R., Zhu, Z., Tanokura, M., Miyakawa, T., and Hachimura, S. (2022). β-elemene regulates M1-M2 macrophage balance through the ERK/JNK/P38 MAPK signaling pathway. Commun. Biol. *5*, 519. https://doi.org/10.1038/s42003-022-03369-x.
74. Feng, W., Liu, H., Luo, T., Liu, D., Du, J., Sun, J., Wang, W., Han, X., Yang, K., Guo, J., et al. (2017). Combination of IL-6 and sIL-6R differentially regulate varying levels of RANKL-induced osteoclastogenesis through NF-κB, ERK and JNK signaling pathways. Sci. Rep. *7*, 41411. https://doi.org/10.1038/srep41411.
75. Hall, J.P., and Davis, R.J. (2002). Inhibition of the p38 pathway upregulates macrophage JNK and ERK activities, and the ERK, JNK, and p38 MAP kinase pathways are reprogrammed during differentiation of the murine myeloid M1 cell line. J. Cell. Biochem. *86*, 1–11. https://doi.org/10.1002/jcb.10187.
76. Johnson, G.L., and Lapadat, R. (2002). Mitogen-activated protein kinase pathways mediated by ERK, JNK, and p38 protein kinases. Science *298*, 1911–1912. https://doi.org/10.1126/science.1072682.
77. Li, M., Hao, B., Zhang, M., Reiter, R.J., Lin, S., Zheng, T., Chen, X., Ren, Y., Yue, L., Abay, B., et al. (2021). Melatonin enhances radiofrequency-induced NK antitumor immunity, causing cancer metabolism reprogramming and inhibition of multiple pulmonary tumor development. Signal Transduct. Targeted Ther. *6*, 330. https://doi.org/10.1038/s41392-021-00745-7.
78. Tang, L., Zhang, C., Yang, Q., Xie, H., Liu, D., Tian, H., Lu, L., Xu, J.Y., Li, W., Xu, G., et al. (2021). Melatonin maintains inner blood-retinal barrier via inhibition of p38/TXNIP/NF-κB pathway in diabetic retinopathy. J. Cell. Physiol. *236*, 5848–5864. https://doi.org/10.1002/jcp.30269.
79. Liu, J., Sun, Q., Sun, M., Lin, L., Ren, X., Li, T., Xu, Q., Sun, Z., and Duan, J. (2022). Melatonin alleviates PM(2.5)-triggered macrophage M1 polarization and atherosclerosis via regulating NOX2-mediated oxidative stress homeostasis. Free Radic. Biol. Med. *181*, 166–179. https://doi.org/10.1016/j.freeradbiomed.2022.02.005.
80. Pita, M.L., Hoyos, M., Martin-Lacave, I., Osuna, C., Fernández-Santos, J.M., and Guerrero, J.M. (2002). Long-term melatonin administration increases polyunsaturated fatty acid percentage in plasma lipids of hypercholesterolemic rats. J. Pineal Res. *32*, 179–186. https://doi.org/10.1034/j.1600-079x.2002.1o851.x.
81. Hou, L., Wang, K., Zhang, C., Sun, F., Che, Y., Zhao, X., Zhang, D., Li, H., and Wang, Q. (2018). Complement receptor 3 mediates NADPH oxidase activation and dopaminergic neurodegeneration through a Src-Erk-dependent pathway. Redox Biol. *14*, 250–260. https://doi.org/10.1016/j.redox.2017.09.017.
82. Yingze, Y., Zhihong, J., Tong, J., Yina, L., Zhi, Z., Xu, Z., Xiaoxing, X., and Lijuan, G. (2022). NOX2-mediated reactive oxygen species are double-edged swords in focal cerebral ischemia in mice. J. Neuroinflammation *19*, 184. https://doi.org/10.1186/s12974-022-02551-6.
83. Arnold, M.E., Slomka, M.J., Breed, A.C., Hjulsager, C.K., Pritz-Verschuren, S.,

Venema-Kemper, S., Bouwstra, R.J., Trebbien, R., Zohari, S., Ceeraz, V., et al. (2018). Evaluation of ELISA and haemagglutination inhibition as screening tests in serosurveillance for H5/H7 avian influenza in commercial chicken flocks. Epidemiol. Infect. *146*, 306–313. https://doi.org/10.1017/s0950268817002898.

84. Bokma, J., Kaske, M., Vermijlen, J., Stuyvaert, S., and Pardon, B. (2024). Diagnostic performance of Mycoplasmopsis bovis antibody ELISA tests on bulk tank milk from dairy herds. BMC Vet. Res. *20*, 81. https://doi.org/10.1186/s12917-024-03927-x.
85. Olaussen, E., and Rekvig, O.P. (1999). Screening tests for antinuclear antibodies (ANA): selective use of central nuclear antigens as a rational basis for screening by ELISA. J. Autoimmun. *13*, 95–102. https://doi.org/10.1006/jaut.1999.0295.
86. Guan, Z., Jin, X., Guan, Z., Liu, S., Tao, K., and Luo, L. (2023). The gut microbiota metabolite capsiate regulate SLC2A1 expression by targeting HIF-1α to inhibit knee osteoarthritis-induced ferroptosis. Aging Cell *22*, e13807. https://doi.org/10.1111/acel.13807.
87. Ye, C., Ho, D.J., Neri, M., Yang, C., Kulkarni, T., Randhawa, R., Henault, M., Mostacci, N., Farmer, P., Renner, S., et al. (2018). DRUG-seq for miniaturized high-throughput transcriptome profiling in drug discovery. Nat. Commun. *9*, 4307. https://doi.org/10.1038/s41467-018-06500-x.

STAR★METHODS

KEY RESOURCES TABLE

REAGENT or RESOURCE	SOURCE	IDENTIFIER
Antibodies		
Anti-IL-1 antibody	Abcam	Cat# ab315084; RRID: AB_3105874
Anti-IL-6 antibody	Abclonal	Cat# A0286; RRID: AB_2757098
Anti-Tnf-α antibody	Abclonal	Cat# A11534; RRID: AB_2758597
Anti-F4/80 antibody	Cell Signaling Technology	Cat# 30325; RRID: AB_2798990
Anti-CD86 antibody	Abclonal	Cat# A16805; RRID: AB_2768800
Anti-CD206 antibody	Cell Signaling Technology	Cat# 24595; RRID: AB_2892682
Anti-Arg-1 antibody	Cell Signaling Technology	Cat# 93668; RRID: AB_2800207
Anti-p-ERK antibody	Cell Signaling Technology	Cat# 5726; RRID: AB_2797617
Anti-p-JNK antibody	Cell Signaling Technology	Cat# 9255; RRID: AB_2307321
594-conjugated Goat anti-Rabbit IgG (H + L)	Abclonal	Cat# AS074; RRID: AB_2768324
Anti-JNK antibody	Cell Signaling Technology	Cat# 9252; RRID: AB_2250373
Anti-p-JNK antibody	Cell Signaling Technology	Cat# 4668; RRID: AB_823588
Anti-ERK antibody	ABclonal	Cat# A4782; RRID: AB_2863347
Anti-p-ERK antibody	ABclonal	Cat# AP0974; RRID: AB_2863871
Anti-iNOS antibody	Cell Signaling Technology	Cat# 13120; RRID: AB_2687529
Anti-Tnf-α antibody	Cell Signaling Technology	Cat# 11948; RRID: AB_2687962
Anti-CD86 antibody	ABclonal	Cat# A19026; RRID: AB_2862518
Anti-IFT27 antibody	MyBioSource	Cat# MBS3208968; RRID: AB_3105920
Anti-GAPDH antibody	Cell Signaling Technology	Cat# 5174; RRID: AB_10622025
Anti-rabbit IgG, HRP-linked antibody	Cell Signaling Technology	Cat# 7074; RRID: AB_2099233
Chemicals, peptides, and recombinant proteins		
Melatonin	Sigma	Cat# M5250
Dimethyl sulfoxide	Sigma	Cat# 34943
Rodent Diet With 60 kcal% Fat	Research Diets	Cat# D12492
Dihydroethidium	Beyotime	Cat# S0063
Fetal bovine serum	Sigma	Cat# F8318
Penicillin-Streptomycin	Gibco	Cat# 15140122
Phenol red cotton threads	Tianjin Jingming New Technological Development	N/A
Oil Red O solution	Servicebio	Cat# G1015,
DAPI	Vector Laboratories	Cat# H-1200-10
Human Dil-Oxidised Low-Density Lipoprotein	Yeasen	Cat# 20609ES76
Lipopolysaccharide	Sigma	Cat# 0111: B4
Anisomycin	Selleck	Cat# S7409
Senkyunolide I	Selleck	Cat# S3275
IL-4	Sigma	Cat# SRP3211
Reverse transcription kit	TaKaRa	Cat# RR036A
SYBR green master mix	Yeasen	Cat# 11200ES03
Phosphatase inhibitor	Thermo Fisher Scientific	Cat# 78420
Phenylmethanesulfonyl fluoride	Beyotime	Cat# ST505
ECL substrate	Millipore	Cat# WBULP-100ML

(*Continued on next page*)

Continued

REAGENT or RESOURCE	SOURCE	IDENTIFIER
Critical commercial assays		
Tissue total cholesterol kit	Applygen	Cat# E1015
Fluid sample total cholesterol kit	Applygen	Cat# E1005
BCA protein quantification kit	Beyotime	Cat# P0012
Deposited data		
Raw and analyzed data for DRUG-seq data	This manuscript	GEO: GSE269343
Experimental models: Cell lines		
RAW 264.7	Shanghai Fuheng Biological Technology	Cat# FH0328
Experimental models: Organisms/strains		
C57BL/6 mice	Beijing Vital River Laboratory Animal Technology	N/A
Oligonucleotides		
IFT27 si-RNA	Genomeditech	N/A
Primers for β-Actin, TNF-α, IL-1β, IFN-γ, IL-4, IFT27, iNOS, CD206, Arg-1, and CD86, see Table 1	This paper	N/A
Software and algorithms		
ImageJ software	ImageJ	RRID: SCR_003070

RESOURCE AVAILABILITY

Lead contact

Further information and requests for resources and reagents should be directed to and will be fulfilled by the Lead Contact, Dr. Yihui Chen (1300089@tongji.edu.cn).

Materials availability

All reagents generated in this study are accessible from the lead contact with a completed Materials Transfer Agreement.

Data and code availability

- Sequencing data have been deposited at gene expression omnibus (GEO) and are publicly available as of the date of publication (GEO: GSE269343).
- All data reported in this paper will be shared by the lead contact upon request.
- This paper does not report original code.
- Any additional information required to reanalyze the data reported in this work paper is available from the lead contact upon request.

EXPERIMENTAL MODEL AND STUDY PARTICIPANT DETAILS

Animals and treatment

Four-week-old male C57BL/6 mice (Beijing Vital River Laboratory Animal Technology Co., Ltd., Beijing, China) were split randomly into two groups and fed either a normal-fat diet (NFD, 10 kcal% fat, $n = 12$) or HFD (60 kcal% fat, Research Diets, Inc., New Brunswick, NJ, USA, $n = 48$). The mice were housed in ventilated cages with alternating 12 h light-dark cycles (8 AM–8 PM) at 25 ± 1°C and 60 ± 10% relative humidity. Six mice in each group were executed at 20 weeks of age in order to verify the effect of HFD on the ocular surface.

MLT was dissolved in dimethyl sulfoxide (DMSO), and the concentrations were adjusted to 10^{-8} M–10^{-3} M (six concentration gradients) with saline, keeping the DMSO concentration at 1%. The remaining mice (NFD $n = 6$, HFD $n = 42$; 20-week-old) were used to verify the therapeutic effect of melatonin eye drops on hyperlipidemic mice. HFD mice were divided into seven subgroups including one control group and six MLT groups (six mice in each group). Saline containing 1% DMSO was administered to the control group and NFD group. MLT at concentrations ranging from 10^{-8} M to 10^{-3} M. For each mouse, 2 μL of solution per eye was administered bilaterally to each mouse at 8:00, 13:00, and 18:00 daily for 4 weeks. The mice were sacrificed at 24 weeks. The ARVO Statement for the Use of Animals in Ophthalmic and Vision Research served as the guide for all animal treatments. The experimental protocol was authorized by the experimental animal ethics committee of Yangpu Hospital, Tongji University (approval number: LL-2022-WSJ-003).

Cell culture and treatment

In an incubator set at 37°C and 5% CO_2, RAW 264.7 murine macrophages (Shanghai Fuheng Biological Co., Ltd., China) were cultivated in DMEM supplemented with 10% fetal bovine solution, 100 U/mL penicillin, and 100 mg/mL streptomycin (supplies sourced from Gibco Life Technologies, Shanghai, China). The RAW 264.7 cells were seeded at a density of 5×10^5 cells/well into a 6-well plate. When the cells reached 70–80% confluency, a serum-free starvation culture was performed for 12 h. The MLT and control groups were defined as RAW 264.7 cells that had been pretreated for 30 min with varying concentrations of MLT (M5250, Sigma-Aldrich) or isochoric DMSO (34943, Sigma-Aldrich), respectively. Next, to induce high lipid and inflammatory conditions in the cells, 100 μg/mL of Ox-LDL (Human DiI-Oxidised Low-Density Lipoprotein, 20609ES76, Yeasen) or 10μg/mL LPS (0111: B4, Sigma-Aldrich) was introduced. An IFT27 knockout lentivirus was constructed by Genomeditech. For lentivirus infection, macrophages (5×10^4 cells per well in a six-well plate) were infected with si-IFT27 or control lentivirus (MOI, 50) in DMEM containing 10 μg/mL polybrene, 10% FBS, and 1% penicillin/streptomycin. To validate this pathway, si-IFT27, 50nM anisomycin (ANI, S7409, SELLECK), and 5μM senkyunolide I (SENI, S3275, SELLECK) were administered 30 min before MLT or DMSO. To induce polarization, RAW 264.7 cells were treated with 10μg/mL LPS (0111: B4, Sigma-Aldrich) for M1 macrophages and 20 ng/mL IL-4 (SRP3211, Sigma-Aldrich) for M2 macrophages after overnight starvation in medium without FBS.

METHOD DETAILS

Plasma and MG cholesterol measurements

Blood, MG, and LG tissues were obtained from mice fed either an HFD or NFD for 16 weeks(20-week-old) after 8 h of fasting ($n = 6$). Serum and meibomian gland total cholesterol levels were determined using a cholesterol assay kit(E1005, E1015, Applygen, China).

Animal examination

The weight of each mouse was recorded weekly. A solitary ophthalmologist used a slit-lamp microscope (Kanghua Science & Technology, China) to examine the corneas and eyelid margins of every mouse every 4 weeks.

Tear secretion test and tear film breakup time

Tear secretion tests and tear film breakup time (TBUT) were performed weekly at 3 PM by a single ophthalmologist.

Phenol red cotton threads (Jingming Co., Ltd., China) were used for the tear secretion test. The tears remaining in the conjunctival sac were dried using absorbent paper before testing. After lightly anesthetized with 1% sodium pentobarbital (50 mg/kg, i.p.), a phenol red cotton thread was positioned at one-third of the distance from the lateral canthus. The wet length of the thread was measured after 1 min and accurate to 0.1 mm.

For the TBUT, the mice's conjunctival sacs were filled with 1 μL of 1% liquid sodium fluorescein (Jingming Co., Ltd., China). Both upper and lower eyelids were squeezed so that fluorescein was uniformly distributed on the ocular surface. The amount of time that passed between the last eye closure and the first disruption in the tear film was recorded. The measurements were performed in triplicate. The average of the TBUT measurements per eye was used in the analysis.

Hematoxylin and eosin staining

MGs and LGs ($n = 6$) were soaked in formalin for 24 h, dehydrated, made transparent, and implanted in paraffin blocks. A total of 5-μm-thick paraffin sections (three sections per animal, six animals per group) were dewaxed, stained, dehydrated, and made transparent. The sections were subsequently sealed so that images could be taken.

Oil Red O staining

The upper and lower eyelids and extra orbital LGs ($n = 6$) were embedded with optimal cutting temperature (OCT) compound and fabricated into 6-μm-thick ice sections. Sections were dipped in Oil Red O (ORO) working solution for 8 min (protected from light) and immersed in isopropanol for 3 s. After rinsing three times with phosphate buffered saline (PBS) for 5 min, the sections were sealed and observed.

Immunofluorescence staining

6-μm-thick cryosections of the MGs and LGs were fixed in 4% paraformaldehyde for 20 min at 25°C. The slices were soaked with 0.2% Triton X-100 for 20 min following PBS washing. After a 60 min incubation period with 2% bovine serum albumin, sections were subsequently incubated for an additional hour at 4°C with anti-IL-1 (1:50, ab315084, Abcam), anti-IL-6 (1:50, A0286, Abclonal), anti-Tnf-α (1:50, A11534, Abclonal), anti-F4/80 (1:200, #30325, CST), anti-IFT27(1:100, MBS3208968, MyBioSource), anti-CD86(1:50, A16805, abclonal), anti-CD206(1:400, #24595, CST), anti-Arg-1(1:50, #93668, CST), anti-p-ERK(1:200, #5726, CST), and anti-p-JNK(1:200, #9255, CST). The sections were coated for 60 min at 25°C with Alexa Fluor 594-conjugated IgG (1:50, AS074, Abclonal) after three consecutive 10-min washes in PBS. Sections were stained with DAPI (Vector Laboratories, Burlingame, USA), and a fluorescent microscope (Olympus, Tokyo, Japan) was used for imaging.

Detection of reactive oxygen species

Hydroethidine, also known as Dihydroethidium, is one of the most commonly used superoxide anion fluorescence detection probes for the detection of reactive oxygen species. The dye can freely enter the cell and is detected by intracellular superoxide anion fluorescence.[81,82]To detect reactive oxygen species (ROS), freshly frozen slices of MGs and LGs were examined under a fluorescence microscope (Olympus, Tokyo, Japan) after 30 min of 10μM dihydroethidium (DHE, S0063, Beyotime, China) staining protected from light conditions at 37°C.

Enzyme-linked immunosorbent assay

Enzyme-linked immunosorbent assay (ELISA)is an immunoassay typically used to measure antibodies or antigens, including proteins or glycoproteins, in biological samples.[83] Like other immunoassays, it relies on the binding of an antibody to a target to facilitate detection.[84,85] The levels of inflammatory cytokines in the supernatant of cells were detected using ELISA kits according to the manual instructions. Shortly, the macrophage supernatant and gradient concentration of standards were added to the well and incubated for 2 h, followed by this addition of biotin antibody, horseradish peroxidase labeled streptavidin, the TMB and the termination solution. The OD values of each well were measured at 450 nm, the concentration curves were plotted and the concentration was calculated.

Molecular modeling and docking of melatonin and IFT27

The docking study of MLT and IFT27 was performed, as committee described.[86] Briefly, the crystal structure of MLT was aligned to the crystal structure of IFT27 by the ChEMBL database (https://www.ebi.ac.uk/chembl/#). CB-Dock software (http://clab.labshare.cn/cb-dock/php/index.php) was used to perform the docking study and the docking results were visualized using the CB-Dock software.

Real-Time quantitative reverse transcription PCR (RT-qPCR)

Hair, skin, muscle, subcutaneous tissue, and conjunctiva were removed from the mouse eyelids under a dissecting microscope, and the MGs were maintained. Each group consisted of three samples, each containing two MGs from the same mouse. After three rinses with PBS, RNA was extracted with the TRIzol reagent. Quantification was performed using a Nanodrop spectrophotometer (Thermo Scientific, Waltham, USA). A reverse transcription kit (RR036A; TaKaRa Bio, Japan) was used to perform reverse transcription with an equivalent volume of RNA. Using SYBR green master mix (11200ES03, Yeasen, China) and a StepOneTM Real-Time PCR detection equipment (Applied Biosystems, USA), RT-qPCR was performed. Table 1 presents the primer sequences for amplification of specific gene products.

The thermal patterns for 40 cycles were as follows: 95°C for 30 s; 10 s of denaturation at 95°C; and annealing and extension at 60°C for 30 s. A melt curve analysis was then performed to verify the specificity of the amplification. Using β-actin as an internal control, the RT-qPCR findings were evaluated using the comparative computed tomography method and standardized against the control group.

Western blotting

Proteins were extracted from the MGs using 1.5% SDS lysis buffer containing a phosphatase inhibitor (cat#78420; Thermo Fisher Scientific, MA, USA) and phenylmethanesulfonyl fluoride (PMSF; ST505; Beyotime, China). The protein concentration was determined using a BCA Protein Quantification Kit (P0012, Beyotime, China). Each group received six samples, each of which contained pooled MGs from both eyes. Next, 20 μg protein in equal parts was taken, separated via SDS-PAGE, and placed onto PVDF membranes (Millipore, Darmstadt, Germany). Following a 2h-blocking period in 5% BSA, the membranes were incubated for an additional night at 4°C using primary antibodies, including anti-JNK (1:1000, #9252, CST); anti-p-JNK (1:1000, #4668, CST); anti-ERK (1:500, A4782, Abclonal); anti-p-ERK (1:500, AP0974, Abclonal); anti-iNOS (1:1000, #13120, CST); anti-TNF-α (1:1000, #11948, CST); anti-CD86 (1:500, A19026, Abclonal); anti-Arg-1 (1:1000, #93668, CST); anti-CD206 (1:1000, #24595, CST); anti-IFT27 (1:100, MBS3208968, MyBioSource); anti-GAPDH (1:1000, #5174, CST); and the secondary antibody (1:1000, #7074, CST). Enhanced chemiluminescence (Millipore, MA, USA) was used to visualize the signals of the identified proteins, and ChemiDoc imaging equipment (Bio-Rad, Hercules, CA, USA) was used to record the images.

Digital RNA with perturbation of genes (DRUG-seq)

The RAW 264.7 cells were grouped into four main categories: control, LPS, MLT, and LPS+MLT. Based on the gradient concentration of MLT, the MLT group and the LPS+MLT group may be further divided into 5 subgroups (10^{-3}M, 10^{-4}M, 10^{-5}M, 10^{-6}M, and 10^{-7}M MLT). Cells treated with different drugs for 12 h were collected for the next step. As previously described,[87] cDNA from individual wells was labeled using DRUG-seq by including certain barcodes in RT primers. Briefly, after the extraction of total RNA using the TRIzol method, DRUG beads and 2x binding buffer were added to capture poly (A) RNA. Single-stranded DNA was obtained through reverse transcription of these products. A Bioptic Qsep100 Analyzer was used to analyze the library. Then, 2x HIFI Amplification Mix and index were added, and PCR Amplification was performed for the library fragments. The DNA beads were screened for library fragments. To determine whether the library size distribution matched with the theoretical size, a Bioptic Qsep100 Analyzer was utilized. The NovaSeq

high-throughput sequencing platform and PE150 sequencing mode were used for sequencing. Data are posted in GEO repository with accession number GSE269343.

QUANTIFICATION AND STATISTICAL ANALYSIS

Means and standard deviations (SDs) are used to present quantitative data. GraphPad Prism (version 6.0; GraphPad Software Inc., USA) was used to process the data. Statistical analyses were performed using the Mann–Whitney U test and one-way analysis of variance. Statistical significance was set at $p < 0.05$.